공학박사 학위논문

Extension of lance life used in the smelting furnace in Mitsubishi process for Cu refining

미쯔비시 동 제련 로에서 Cu 제련 공정에서
사용하는 랜스 수명 연장에 대한 연구

2021 년 2 월

서울대학교 대학원

재 료 공 학 부

임 성 미

Extension of lance life used in the smelting furnace in Mitsubishi process for Cu refining

지도 교수 이 경 우

이 논문을 공학박사 학위논문으로 제출함

2021 년 2 월

서울대학교 대학원

재 료 공 학 부

임 성 미

임성미의 공학박사 학위논문을 인준함

2021 년 2 월

위 원 장 황 농 문 (인)

부위원장 이 경 우 (인)

위 원 차 필 령 (인)

위 원 남 호 석 (인)

위 원 이 중 의 (인)

Abstract

Extension of lance life used in the smelting furnace in Mitsubishi process for Cu refining

Lim sung mi

Department of Materials Science and Engineering

The Graduate school

Seoul National University

Smelting is the first step in the Mitsubishi continuous process for Cu production, resulting in the production of 68% copper matte and Fe-silicate slag. One of the main issues pertaining to the smelting furnace is the frequent interruption of operations required to allow the inspection and replacement of lances since lances are frequently fractured.

First, the present study was aimed at modifying the operating conditions of the smelting furnace to suppress lance fractures. A numerical model was developed to simulate the transport phenomena including multi-phase behaviors in the furnace. The simulation results showed that the lances were exposed to a

severely erosive atmosphere with high temperatures. Further calculation indicated that raising the positions of the lances could lower the temperature of the lances, and reduce the occurrence of splashed melt, which contains erosive sulfides. This condition was applied and observed in the field operation. It was confirmed that by implementing such a change of the lance heights, the occurrence of lance failures had been considerably reduced without notably affecting the reaction ability of the smelting furnace. Additionally, modifying the feeding system was suggested that feeding continuously as a method of stabilizing the interior of smelting furnace during the process because the effective reactivity could be increased. Second, investigation of lances used in field operations, thermodynamic analysis and laboratory experiments were conducted for studying the reaction mechanism. By analyzing the lances, the surface of the lances was damaged and penetration of matte components into the lance was observed and the damage occurred to a certain height. Since the lance temperature varies depending on the height, we could estimate that damage on the lance is directly related to the temperature. Therefore, thermodynamics calculations were conducted and Cu-Fe alloy existed as a liquid phase at approximately 1100°C. Based on the experimental results, laboratory experiments were conducted and liquid copper was also produced at above 1100°C. From these results, it can be considered that temperature above 1100°C can cause the lance fracture and part of the lance located at higher temperature than 1100°C can be deteriorated and finally fractured. Thus, during the Mitsubishi process, when the lance is kept at a temperature below 1100 in the furnace, surface damage can be reduced and the lance life-time can be increased.

Through the present study, a numerical model within the S-furnace was developed and we suggested conditions to reduce the fracture of lance using this model. From microstructure analysis of lance, we found out the mechanism by which lance fracture occurs, and confirmed that maintaining the lance tip below 1100℃ can result in stable conditions for increasing lance life-time.

Keywords: Smelting furnace, thermodynamics analysis, surface erosion of high Cr steel, fracture of lance, Cu penetration phenomena

Student number: 2014-22528

Contents

List of Figures

List of Tables

Chapter 1. Introduction

1.1. Smelting furnace in Mitsubishi continuous process

Mitsubishi continuous process is a method of refining copper from copper ores, which consists of three furnaces: the smelting furnace for matte production (S-furnace), the electric slag cleaning furnace for matte/slag separation(CL-furnace) and the converting furnace for copper crude metal production(C-furnace). The Mitsubishi process is being implemented in Naoshima in Japan, Timmins in Canada, Dahej in India and Onsan in South Korea. In the smelting furnace, dried concentrates, fluxes and recycled materials are injected into molten bath with oxygen-rich air through vertical lances. The copper concentrates are instantly smelted and thus produce high grade of matte which around 68% copper and Fe-silicate slag [1]. The feed materials penetrate into bath and rapidly melt due to the effective heat transfer in turbulent area of the melt. Oxygen reacts with the iron sulfide in the matte and oxidized iron combines with flux to form slag [2]. In the process, the matte and slag stay molten state during tapping and transfer. The surface tension of Cu_2S-FeS mattes ranges from 0.33-0.45 N/m. Specific gravity ranges linearly from 3.9 for pure FeS to 5.2 for pure Cu_2S. Interfacial tension increases from near zero in low copper matte to about 0.3 N/m for high copper matte. (~70 mass% Cu_2S) [3]

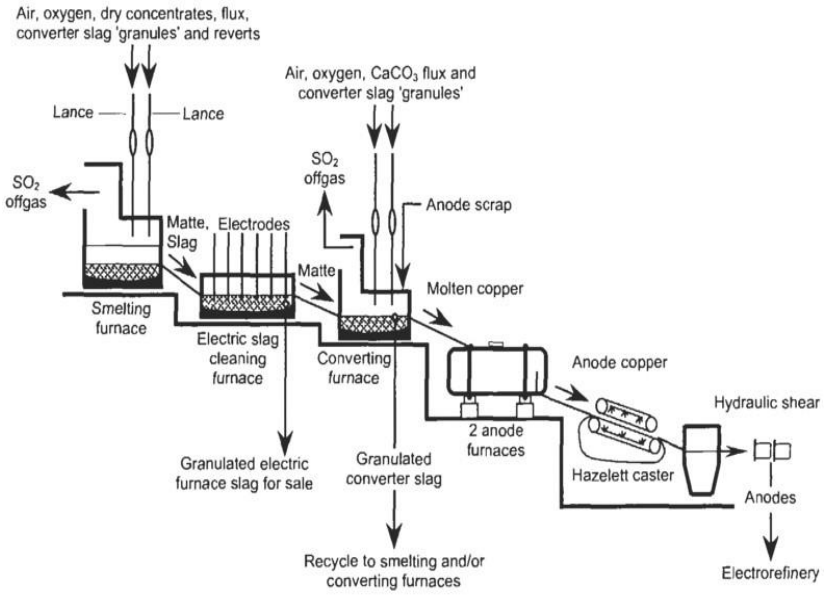

Fig. 1 Mitsubishi process flow sheet [1]

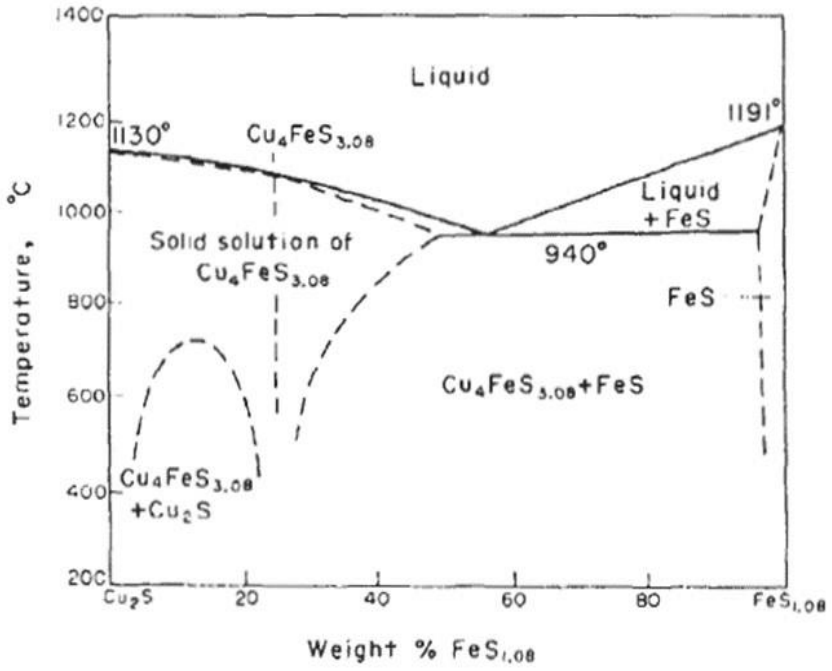

Fig. 2 Cu_2S-FeS(matte) phase diagram. [1]

The main purpose of smelting furnace is to transfer the sulfide minerals in copper concentrate to three components: matte, slag and off-gas. It is acquired

by reacting sulfide minerals with oxygen. The initial reaction follows the form of the following equation,

$$CuFeS_2 + O_2 + SiO_2 \rightarrow (Cu\text{-}Fe\text{-}S)_{matte} + (FeO\text{-}SiO2)_{slag} + SO_2\,(g) \qquad (1)$$

The off-gas containing SO_2 is generated by the smelting reaction. The strength of the off-gas is usually 10 ~ 60 vol% SO_2. The off-gas contains substantial amount of dust up to 0.3 kg/Nm3. This dust is formed from small particles of unreacted copper concentrate of flux, droplets of matte and slag which did not settle into matte layer and volatilized elements in the copper concentrate such as Sb, Bi and Pb. The dust contains 20-40% Cu thus it is important to recycle dust to maintain a constant level [3].

1.2. Fracture of lance

One of the issues which hinder smelting process is irregular wearing down of lances through which copper concentrate, oxygen and fluxes are injected into the top of the melt. Lances are made of a high Cr steel which shows good resistance to corrosion and oxidation, as well as excellent weld-ability, but still the life time of lances is momentary [5]. However, irregular fracture of the lances frequently occurred during process as shown in Fig. 3. During the process, the tip of the lance is suggested to be kept at a fixed height. So the top of the lance was welded and the tip of the lance was aligned through visual inspection when process was stopped. Irregular lance fracture causes increased consumption of the lance, frequency of inspection and replacement cost of the lance. Because replacement of the lance costs more than 10 billion a year. Because of the interruption to process, the cost of process increases and negative impact on furnace efficiency can be made. Also, impact propagates on CL furnace and C furnace. The exact reason for this phenomenon has not been clearly revealed yet.

Fig. 3 Fractured lances after actual processing

1.3. Previous studies for the smelting furnace

Previous researches are mostly reviewing paper which analyze the Mitsubishi process. The previous simulation researches studies not on the analysis of entire lance system, but on one or two lance system. And previous researchers focused on the lancing system of the Mitsubishi process to solve the refractory erosion problem. E. Kimura et al investigated the lancing mechanism in a Mitsubishi smelting furnace with examining the characteristics of a jet of gas-solid mixture using a cold model and an equation that is able to estimate the penetration depth of the solid [1]. Among reported papers by LS-Nikko Copper's researchers, S. S. Park and J. S. Jang investigated the penetration behavior of the annular gas-solid jet into a liquid bath by measuring the penetration depth and compared it with the circular jet behavior and the effects of the physical properties of solid particles on the penetration behavior of a gas-solid jet injected into the liquid bath for both circular and the annular lances [6][7] Several studies with simulation focused on analyzing entire systems of the furnaces for other copper smelting processes. In 1990, Y. B. Hahn and H. Y. Sohn developed a mathematical model for the flash smelting process using TEACH code, SIMPLER algorithm and PSI-CELL technique [8]. The model was verified to describe various important aspects well for the phenomena occurring in the flash smelting furnace. M. Nagamori et al developed a comprehensive thermodynamic simulation model for the Isasmelt process by combining the heat balance of 48 constituent species and the equilibrium mass balance regarding Aksoy's reaction in 1994 [9]. The model enables systematic evaluation of an operating condition, and provides a diagnosis of commercial

furnace performance. Xin-feng and T. Xiao employed numerical simulation for the purpose of optimizing the product in a flash smelting furnace in 2003 [10]. Many reports have investigated the general fracture behavior of high Cr stainless steels. Young and Watson (1995) investigated corrosion at high temperatures [11] and Asteman et al. investigated the effect of temperature on Cr evaporation in stainless steel. [12] In addition, Sahlaoui et al. (2004) developed a model about depth of inter-granular corrosion. [13]

Nonetheless, it is hard to find studies on the fracture behavior of smelting furnace lances. Therefore, the main cause of fractures of lances in smelting furnace is less known. Therefore, the main cause for fracture of lances in smelting furnaces should be suggested.

Chapter 2. Numerical modeling

2.1. Explanation about model

The investigation of heat transfers and flow field using experimental measurements in Mitsubishi smelting furnace is hard due to high temperature severe reaction in the furnace. Therefore, the numerical simulation has achieved its usage as detailed data could be obtained. Numerical model was developed using a commercial package, ANSYS-FLUENT 18.2 and almost 2milion hexagonal grids are adopted. The grid system is shown in the Fig. 4 and LS NIKKO.Co supported the size of model. The diameter of the furnace is 10.1m, the height is 4.0m and the initial matte height is 1.35m with a slag height of 150mm. The total melt height is 1.50m.

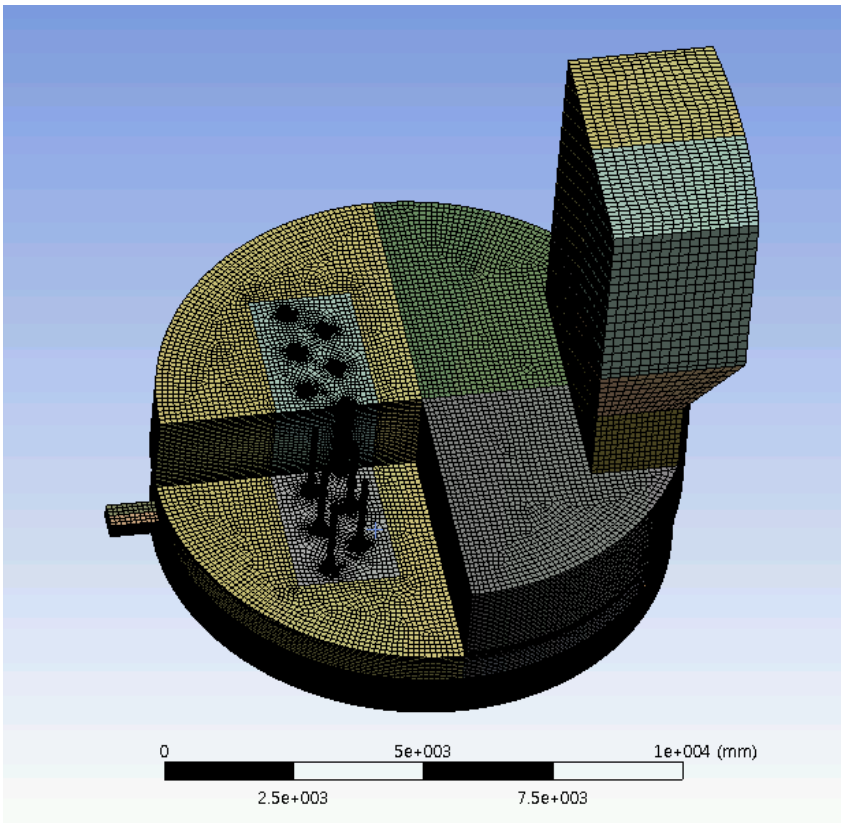

Fig. 4 Grid configuration of smelting furnace.

2.2. Governing equation

The governing equations of the mass and momentum conservation used in the model and the shear stress, Reynolds stress are given as follows.

Mass conservation equation is

$$\nabla \cdot \mathrm{U} = 0 \tag{2}$$

where U is the velocity field (m/s).

Momentum conservation equation is

$$\frac{\partial \rho_m U}{\partial t} + \nabla \cdot (\rho_m UU) = -\nabla P + \nabla \cdot (\tau + T^t) + \rho_m g + f_\sigma \tag{3}$$

where ρ_m is the density (kg/m^3), P is pressure (Pa), g is the gravity (m/s^2) and f_σ is the force per unit volume.

Shear stress, τ is given by

$$\tau = \mu_m \left[(\nabla U + \nabla U^T) - \frac{2}{3} \nabla \cdot U \right] \quad (4)$$

where $\mu_m$is the dynamic viscosity (kg/m·s).

Reynolds stress, $T^t$is given by

$$T^t = \mu_t \left[(\nabla U + \nabla U^T) - \frac{2}{3} \nabla \cdot U \delta_{ij} \right] - \frac{2}{3} \rho_m k \delta_{ij} \quad (5)$$

where μ_t is the turbulent viscosity (kg/m·s), k is the turbulent kinetic energy (m^2/s^2), and $\delta_{ij}$is the Kronecker delta.

Turbulence is calculated by realizable k-ε turbulence model that has an advantage in modelling strong streamline curvature [14]. The governing equations of turbulence parameter are given as follows. Turbulence kinetic energy (k) equation is

$$\frac{\partial}{\partial_t} (\rho_m k) + \nabla \cdot (\rho \mathrm{ku}) = \nabla \cdot \left[\left(\mu + \frac{\mu_t}{\sigma_k} \right) \nabla \cdot k \right] + G_k + G_b - \rho_m \varepsilon - Y_M \quad (6)$$

where G_k is the generation of turbulence kinetic energy (m^2/s^2) due to the mean velocity gradients and G_b is the generation of turbulence kinetic energy (m^2/s^2) due to buoyancy. Y_M represents the contribution of the fluctuating expansion in compressible turbulence to the overall dissipation rate (m^3/s^3).

Turbulence dissipation (ε) equation is

$$\frac{\partial}{\partial t}(\rho_m \varepsilon) + \nabla \cdot (\rho_m \varepsilon u_j) = \nabla \cdot \left[\left(\mu + \frac{\mu_t}{\sigma_\varepsilon}\right) \nabla \cdot \varepsilon\right] + \rho C_1 - \rho C_2 \frac{\varepsilon^2}{k+\sqrt{v\varepsilon}} + C_{1\varepsilon} \frac{\varepsilon}{k} C_{3\varepsilon} G_b \quad (7)$$

Turbulent viscosity (μ_t) is

$$\mu_t = \rho_m C_\mu \frac{k^2}{\varepsilon} \quad (8)$$

$C_{1\varepsilon}$, C_2, σ_k, σ_ε are 1.44, 1.9, 1.0, 1.2 respectively [14].

Molten matte, liquid slag and gas phase co-exist in the furnace. The volume fractions of each phase were calculated using VOF (Volume of Fluid) model. The interface between gas and liquid in the VOF model are discontinuous at the interface, and can be calculated by the scalar transport equation of the phase indicator field. For the case of non-compressed flow, the volume fraction of the phase i in question can be obtained by the following equation.

$$\frac{\partial \alpha_i}{\partial t} + \nabla \cdot \alpha_i U = 0 \tag{9}$$

α_i refers to the liquid phase volume fraction.

Behavior of injected particles were modelled by DPM (Discrete Phase Model) methods [14]. The path of a particle in a discrete phase is calculated by the particle's force balance in Lagrangian frame which is described mathematically as follows.

$$\frac{du_p}{dt} = F_D\left(u - u_p\right) + \frac{g_x(\rho_p - \rho)}{\rho_p} + \frac{\rho}{\rho_p} u_p \frac{\partial u}{\partial x_i} \tag{10}$$

$$F_D = \frac{18u}{\rho_p d_p^2} \frac{C_D Re}{24} \tag{11}$$

$$\mathrm{Re} = \frac{d\rho p|u_p - u|}{\mu} \tag{12}$$

$$C_D = a_1 + \frac{a_2}{Re} + \frac{a_3}{Re^2} \tag{13}$$

where $u_p$is the particle velocity (kg/m·s), u is the fluid phase velocity (m/s), μ is the molecular viscosity of the fluid (kg/m·s), ρ is the fluid density (kg/m^3), ρ_p is the density of the particle(kg/m^3), d_p is the particle diameter (m), F_D is the drag force (N), and C_D is the drag coefficient. During calculation, particle phases and continuous phases are coupled, and exchange of mass, heat and momentum between two phases take place.

$$S_m = \frac{\Delta m_p \dot{m}_{p,0}}{m_{p,0}} \tag{14}$$

$$F_i = \sum \left[\frac{18u}{\rho_p d_p^2} \frac{C_d Re}{24} (u - u_p) + \frac{g_x(\rho_p - \rho)}{\rho_p} + \frac{\rho}{\rho_p} u_p \frac{\partial u}{\partial x_i} \right] \dot{m}_p \Delta t \tag{15}$$

where S_m is the mass exchange(kg) from the discrete phase to the continuous phase, Δm_p is the particle mass change in each control volume(kg), m_p is the mass flow rate of the particles(kg/s), $m_{p,0}$ is the initial mass flow rate of the particles(kg/s), and F_i is the momentum transfer. Additionally, we applied effective heat capacity for considering latent heat of the particles. The value of heat capacity was set according to piecewise-linear profile taken from previous studies [15]. The heat transfer in the furnace is defined by solving the governing equation.

$$\rho C_p \nabla \cdot (vT) = k_{eff} \nabla^2 \cdot T + S + q_{rad} \quad (16)$$

where ρ is the mass density (kg/m^3), T is the temperature (K), k_{eff} is the effective thermal conductivity of the fluid flow (W/m·K), S is heat source generated by reactions. In the present study, we assumed that the following reaction arises in the smelting furnace [1].

$$CuFeS_2 + O_2 + SiO_2 \rightarrow (Cu\text{-}Fe\text{-}S)_{matte} + (FeO\text{-}SiO2)_{slag} + SO_2\,(g) \quad (19)$$

Heat generation was calculated with a thermodynamic calculation program FACTSAGE. The reaction did not combine with the present 3-D simulation. Instead, the calculated values of generated heat were given at the area (heat zone) where gas jet touched the melt. The amount of heat generation was assumed to be proportional to the supplied oxygen value obtained by LS-Nikko co.

2.3. Calculation conditions

The temperature of the injected gas through the lance is assumed 25°C, with a velocity of 125m/s. The initial temperature of the matte, slag and gas is 1250°C. [5]. The lance has an outer diameter of 101.56mm and a thickness of 5.6mm. Eleven lances were placed on top of the melt. The physical properties of the matte, slag and gas are given in Table 1. Furthermore, for the S furnace, the injection materials are injected at high velocity(125m/s), which results in strong mixing. So it can be deduced that matte and slag are fully mixed. So it could be considered that a mixture with the fractions are to be values listed in Table 2. Furthermore, the composition of lance is shown in Table 3. [11]

	Melt	Lance	Matte	Slag	Gas	Refractory
Density (kg/m^3)	4,080	7674.2	4,887	3,650	1.257	3,160
Viscosity (kg/m-s)	0.0537	-	0.0100	0.0770	0.0000192	-
Specific heat (J/kg-K)	934	586.2	587	1181	952	1,175
Thermal conductivity (W/m-K)	17	31.5	-	-	0.0265	3.25

Compositions of Gas: 73 vol%O_2, 27 vol%N_2 (300K)

Table 1 Physical properties

	App. Quantity		Volume fraction	Weight fraction
Matte	54.0 t/h	11.0 m^3/h	0.35	0.42
Slag	75.8 t/h	20.8 m^3/h	0.65	0.58
Total	129.8 t/h	31.8 m^3/h	1	1

Table 2 Ratio of matte and slag

Chemical Composition	Si	S	Cr	Mn	Fe	Ni	Mo	C
in wt%	<1.0	<0.01	27.3	<0.1	65.8	4.3	<0.5	<0.5

Table 3 Chemical composition of lance

2.4. Heat source

FACT-SAGE was used to compute thermodynamics and then put in enthalpy values. The reaction condition is the same as the actual process and calculated as the main equation $CuFeS_2 + O_2 + SiO2 \rightarrow (Cu\text{-}Fe\text{-}S)_{matte} + (FeO\text{-}SiO2)_{slag} + SO_2$ (g) . By calculation, the reaction enthalpy per 100g of concentrates is 4.69e+05 J. In this process, total feed rate is 52kg/s. (2.44e+08 J/sec) But we considered only the remaining values from the amount of heat generated by the injection material, except the heat that goes out with the matte and slag (1.39e+08J/sec). [19] Furthermore, we except the heat conducted to the wall or dust (2.32e+07J/sec), because we developed only S-furnace in this model. (Except next process in Mitsubishi continuous process) The heat source region was considered as much as the volume of the cavity area that was created when injection material was injected. When the height of lances is 0.7m, the volume of cavity is 2.67m^3 and in 1.5m condition, volume is 1.73m^3.

But in heat source calculation, because of constant total feed rate which means total heat is constant, so heat generation per unit volume was applied differently according to the conditions. because the depth of cavity is different in each height conditions. As a result of reflecting all of these considerations, when the height of lances is 1.5m, 3.06e+07J/m^3-s will be heated from source-term is 1.5m and 4.72 e+07J/m^3-s when the height of lance is 0.7m.

Chapter 3. Result of Computational analysis

3.1. Condition 1: Height of lance from melt surface

3.1.1 Results of computational analysis

With the initialization of the calculation, the velocities of the melt increased rapidly, and the average values tended to oscillate within a limited range after 40 s, as shown in Fig.5. Thus, the analysis for the calculated data was performed from this time. From the results, a decrease in the momentum transfer from the gas to melt led to a decrease in the melt velocities, which may suppress the mixing in the melt. This mixing is critical because the reactions mainly occur in a limited region under the lance; consequently, the injected materials should be reacted with all of the melt, and unreacted melts are required be supplied by convection. Because the melt is strongly agitated, the convection is likely the main mechanism of the mixing in a smelting furnace. This means that the average melt velocity can be used as an index for the mixing of the melt. At a height of 1.5 m, the mean velocity of the melt was 0.09 m / s, which is 35% lower than the rate of 0.14 m / s pertaining to a height of 0.7 m. This change likely occurs because the momentum from the gas and injected particles to the melt decreases owing to the increase in the distance from the lance tip to the melt. Consequently, the melt volume fractions in the gas region decreased, as shown in Fig 6.

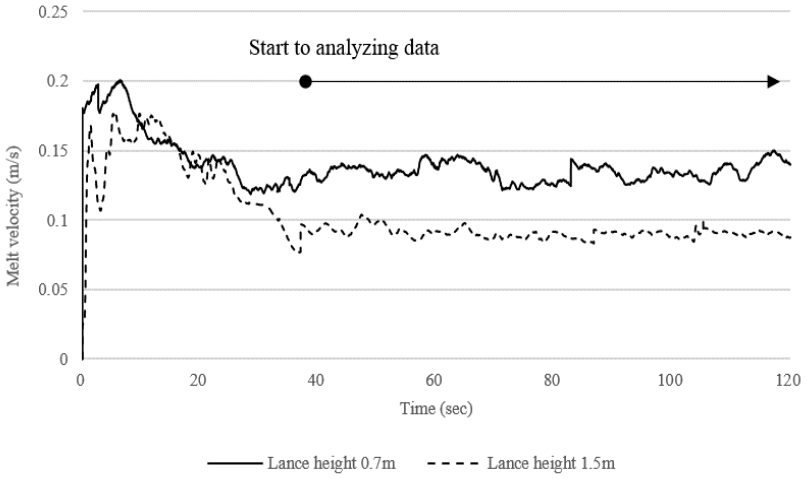

Fig. 5 Change of volume average value of melt velocity during calculation

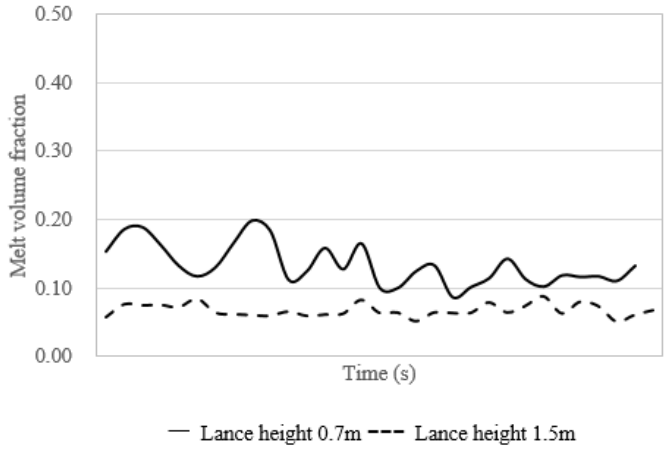

Fig. 6 Melt splash in air region vs time

To understand the effects of lance lifting, the results when the lance height was 1.5 m were compared to those pertaining to a lance height of 0.7 m. By raising the lance to 1.5 m, the cavities became shallower, as shown in Fig 7. The definition of penetration depth in this study is the depth of melt produced by the injection material. However, quantitative figures are not provided to indicate the depth or percentage of a specific substance. In the current result of CFD, criteria are required to analyze penetration depth, and we defined and compared the depth range from one point to the zero end of the air under the mat surface (Melt volume fraction=1 to 0) penetration depth. Each penetration depth was calculated in Fig.8. The average penetration depth for this lance height was 0.35m compared to the value of 0.54m for a lance height of 0.7 m. This distribution occurs because the momentum from the injected gas and particles to the melt decreases owing to the increase in the distance from the lance tip to the melt. However, decrease in the convection does not directly means that the decreased mixing ability pertaining to a larger lance height is insufficient to achieve a sufficient amount of reaction for the smelting furnace, because this sufficient amount has not been conclusively determined. Therefore, we attempted to determine the ability of mixing by measuring the weak-acid concentration in both the original and modified conditions in 3.1.3.2.

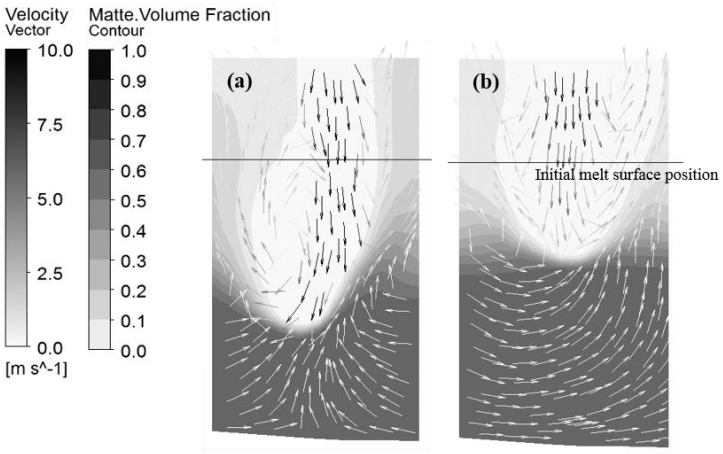

Fig. 7 Penetration depth (a) 0.7m, and (b) 1.5m

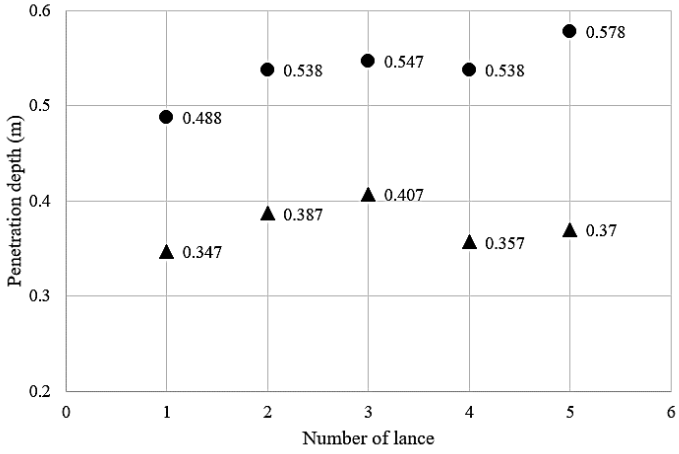

Fig. 8 Penetration depth under each lance with different height

The temperature profiles along the positions of the lance, as shown in Fig. 9, suggest that the lance temperatures can be decreased by increasing the lance height. The x-axis of this graph represents the distance from the lance tip. Since the heat of reaction is generated in the area where the cavity is formed, the lance temperature is higher as the positions are closer to the melt. For a lance 0.7 m from the surface of the melt, the temperature at the end of the lance is above 1160 ° C in this calculation conditions shown in Fig.10. To understand the effects of the lance height, several calculations were performed at different lance heights. It was found that by increasing the lance height, the temperature of lance during the operations decreased. The lances may be attacked by splashed melt droplets because melt droplets exist near the lance. Because melt contains high concentrations of sulfur, lances are exposed very erosive environments. And the high temperature with severely erosive environment was believed to accelerate metal corrosion.

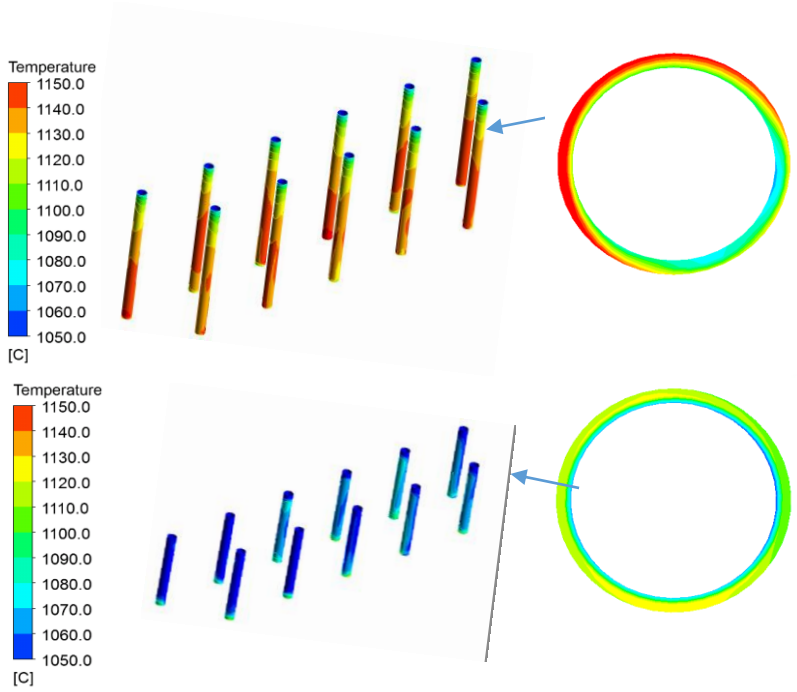

Fig. 9 Image of lance temperature distribution

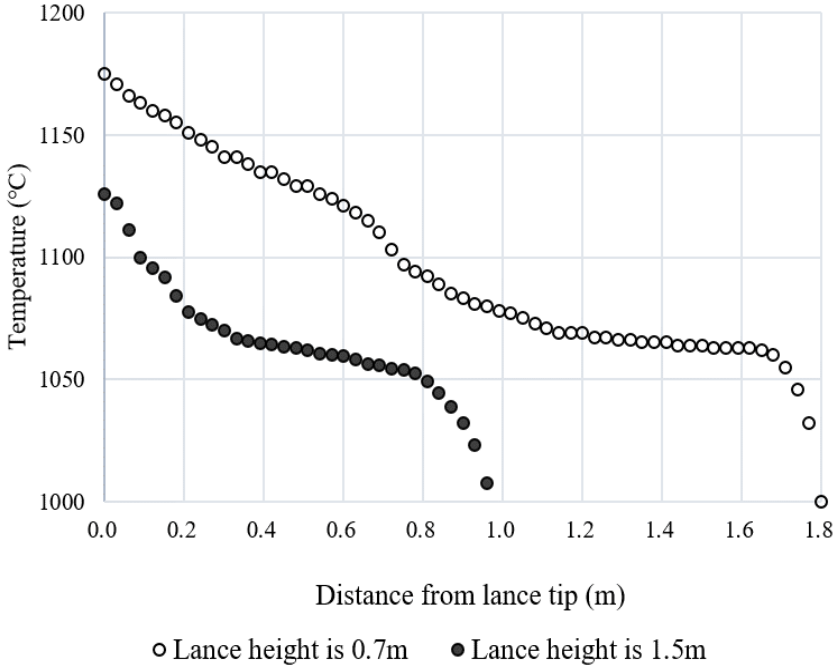

Fig. 10 Lance temperature distribution

3.1.2 Microstructural analysis of lance surface

Height of lances have been changed in field operation and the process was executed for several months. We investigated cross sections of lances used in each operating conditions. Samples of the lance used in the different conditions were obtained, and their cross-sections were investigated. Sample 1 was obtained from a lance operating at a lance height of 0.7 m for an operation time of 16 h. Sample 2 was obtained from a lance operating at a lance height of 1.5 m for an operation time of 12 h. Because of the severe conditions existing in the smelting furnace, samples with the same operation duration could not be obtained. Fig.11 shows the shows the surface electron microscopy image and the energy-dispersive X-ray spectroscopy (EDS) results for sample 1. Figure 12 shows the corresponding images for sample 2.

In the figures, the right side corresponds to the outer side of the lance, which was exposed to the severe furnace atmosphere and was thus more damaged than the inner side. EDS was used to analyze the composition of the specimen, and the degree of damage of each sample was compared. Because Cr is known to be easily evaporated from high chromium steel in high temperature environments, [21] we compared the concentration of Cr in each specimen. (Fig.13 and15) Because the concentration of Cr in the lance used in the smelting furnace is approximately 27% [22], the depth from the surface to the position at which the Cr concentration is lower than 27% was measured and termed as the ‘damage depth’ (Figs. 14 and 16). In Figure 14, the region with

high chrome concentrations on the surface pertains to the chrome oxide produced on the lance surface. [23] Therefore, we considered the position at which the Cr concentration sharply decreases as the starting point for measuring the damage depth.

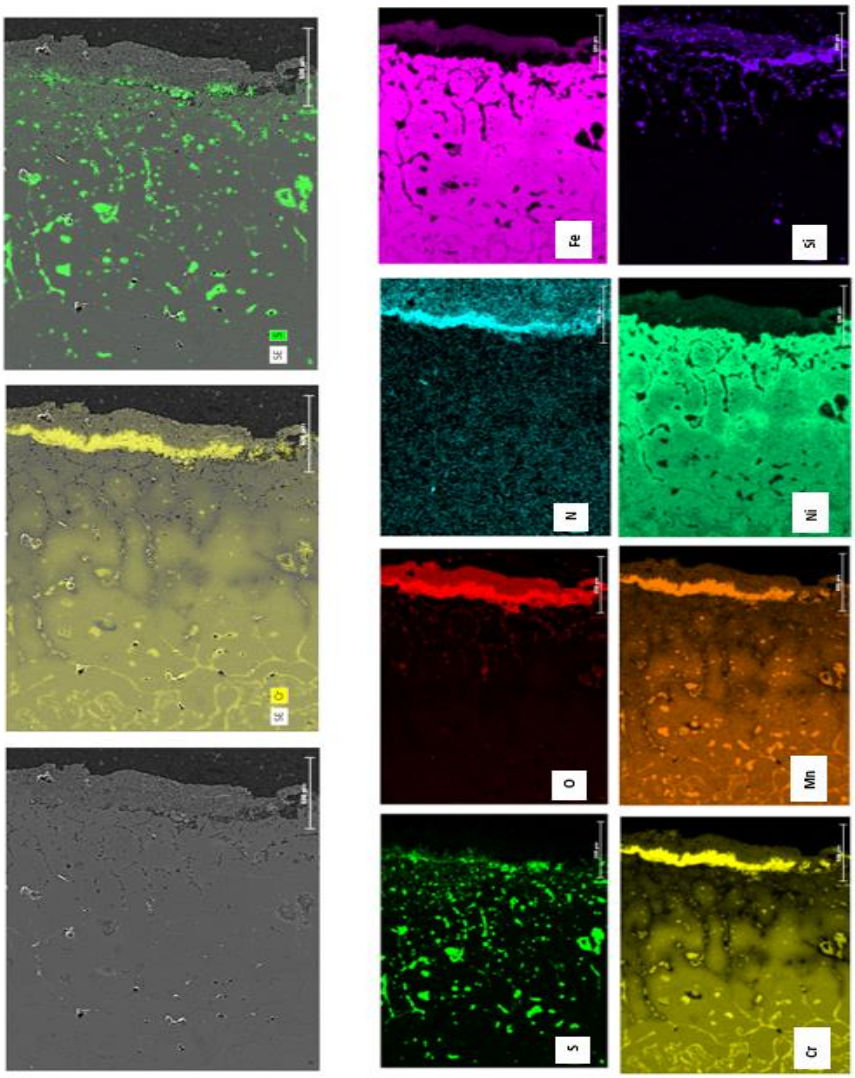

Fig. 11 Microanalysis images in lance height 0.7m

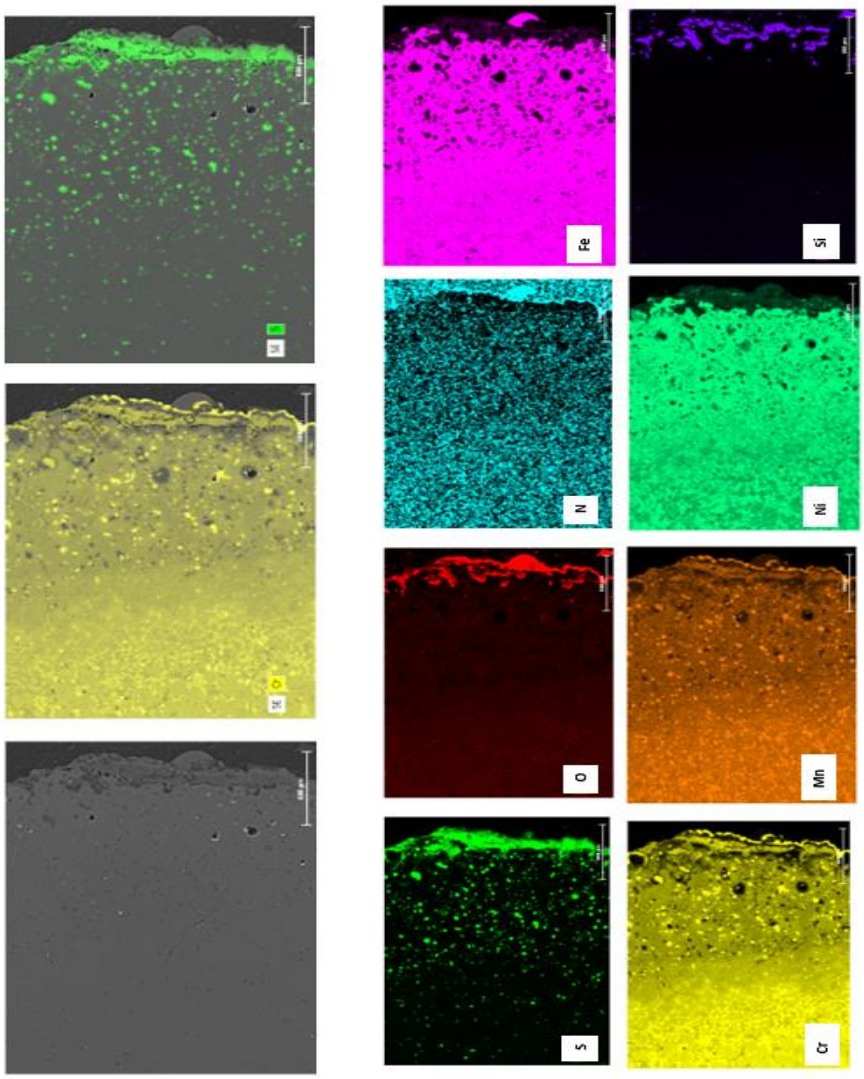

Fig. 12 Microanalysis images in lance height 1.5m

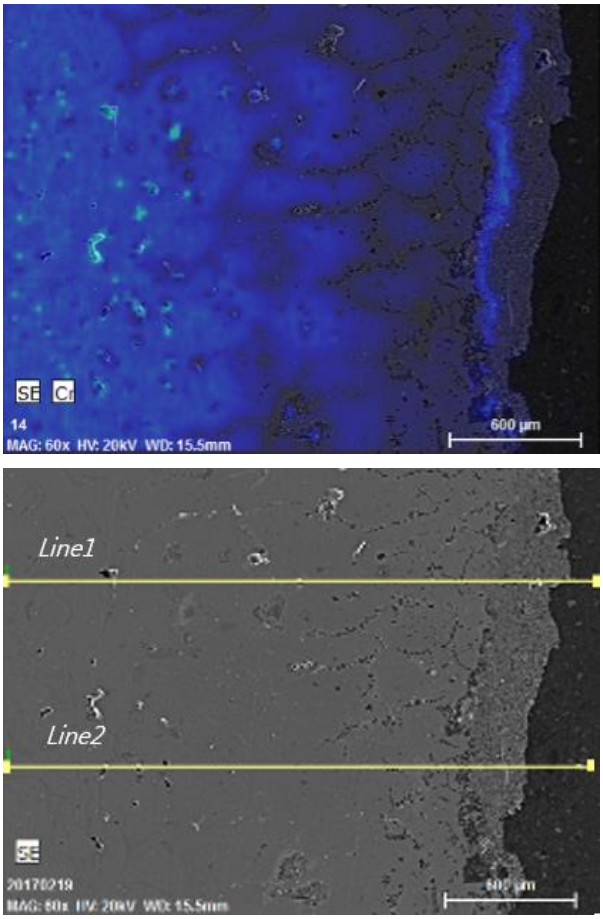

Fig. 13 Microanalysis images in lance height 0.7m of SEM image of lance, and EDS composition map of Cr

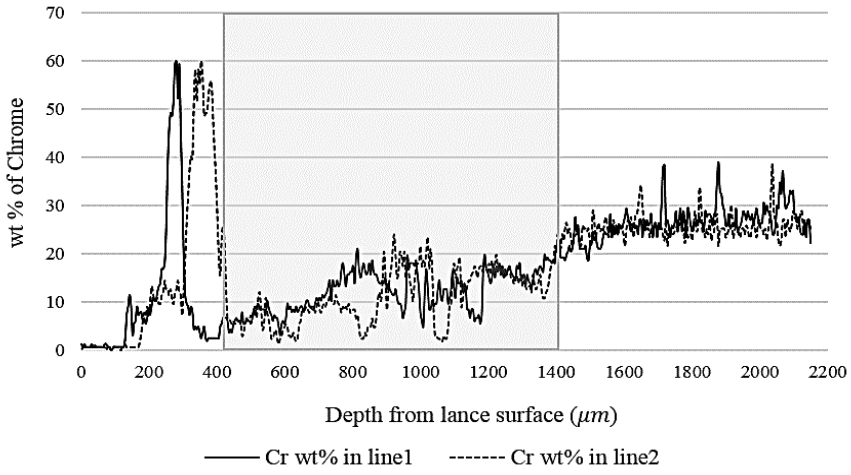

Fig.14 Chrome concentration in lance height 0.7m

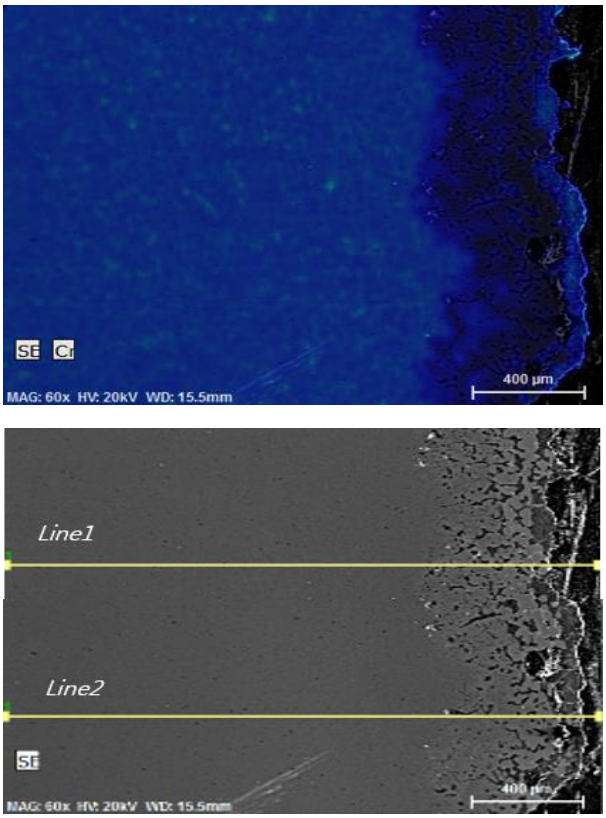

Fig. 15 Microanalysis images in lance height 1.5m of SEM image of lance, and EDS composition map of Cr

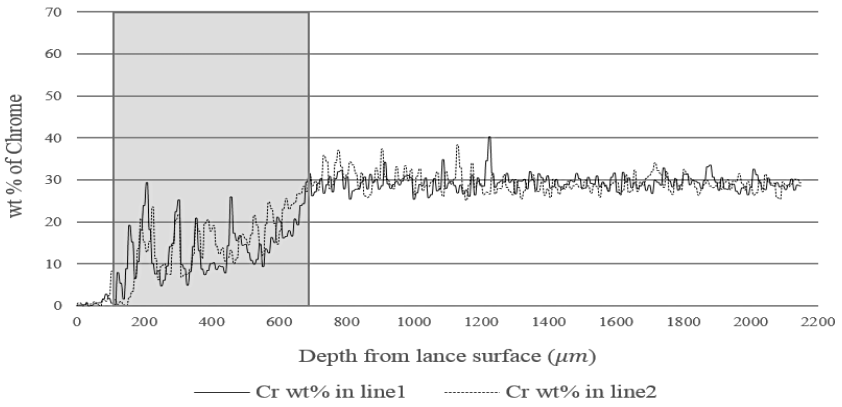

Fig. 16 Chrome concentration in lance height 1.5m

We measured the depth of the entire area in each sample and calculated the mean value. The average damage depth of samples 1 and 2 was 1100μm (Fig. 14) and 600μm (Fig 16), respectively. In general, the relation between the time and reaction thickness depends on the reaction controlling step.

The reaction may occur at the surface of lances. To occur the reaction, Cr should diffuse to surface and at the surface, Cr reacted with O or S_2. So the reaction rate may be controlled by diffusion or reaction. The reaction thickness kinetics is classified into diffusion-controlled or reaction-controlled. In the diffusion-controlled case, the thickness formed increases proportionally to the square root of time, $x = \sqrt{k_D t}$ where k_D is the rate constant for diffusion [24]. The ratio of square root of time for sample 1 to 2 is 1.154 and the ratio of thickness of damaged region of sample 1 and sample 2 is 1.928 which is greater than the value (1.154) of diffusion control. And in the reaction-controlled case, the relation is $x = k_g t$ where k_g is the rate constant for diffusion [24]. The ratios of time for sample 1 to 2 is 1.333 and also lower than experimental value of 1.928. In this case, reaction rates of sample1 should be higher than that of sample2. And this results can be explained of we assume that temperature of sample 2 is lower than that of sample1 as predicted by the numerical simulation. (Fig.9 and 10)

3.1.3 Results of process application

3.1.3.1. Consumption of lance

To determine effect of changing lance height in field operation, we recorded the number of lances consumed. Because fractured lances are replaced during inspection, the number of lances consumed reflects the frequency of lance failure. The data of lance consumption showed that raising the lance height could successfully decrease the lance failure. Fig. 17 shows the change in the number of lances consumed before the modification to that after the lance height was changed. The lance average consumption was reduced by nearly 50% when the lance height was increased shown in Fig.18.

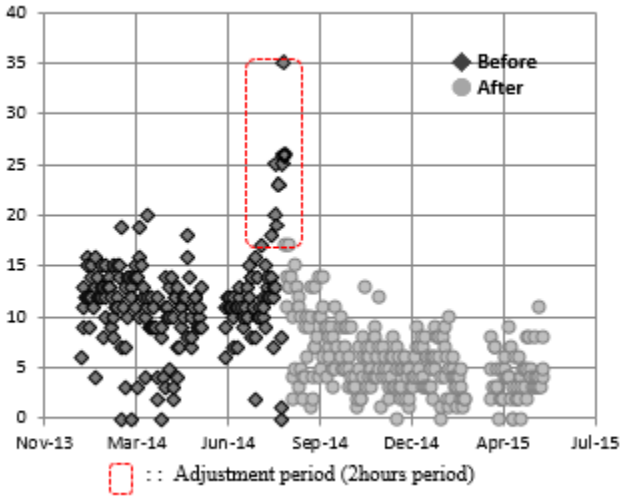

Fig. 17 Daily consumption of lance

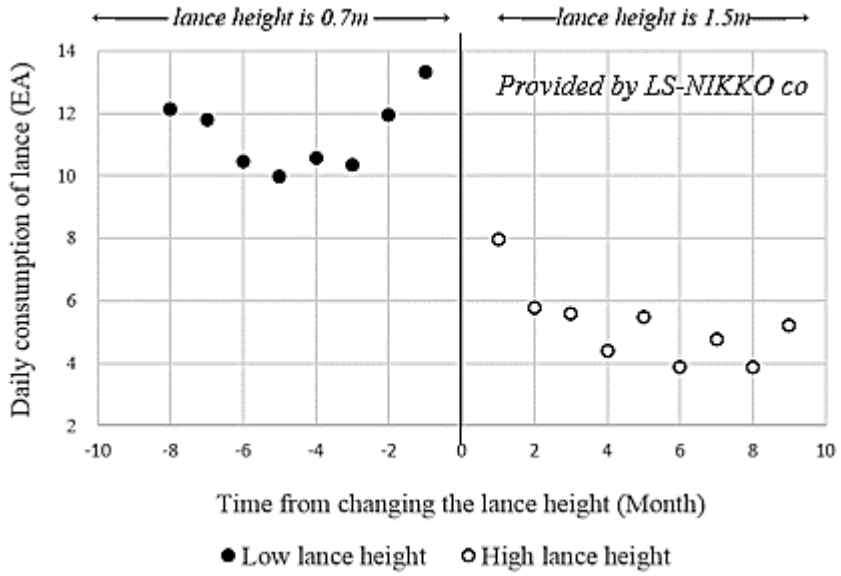

Fig. 18 Monthly average of daily consumption of lance

3.1.3.2 Concentration of weak acid

Above mentioned that decrease in the convection does not directly mean that the decreased mixing ability. Therefore, we attempted to determine the ability of mixing by measuring the weak-acid concentration.

The weak acid concentration was used as the index to demonstrate the ability of mixing in the furnace for the following reason. The main reaction in the smelting process involves the Cu concentrate consisting of Cu and the Fe-sulfide reacting with oxygen to generate Fe-oxide and matte and SO_2 gas is generated. (Eq. 1) Matte making reaction occurs at the cavity area which O_2 and sulphides meet and react. Because oxygen is continuously suppled to this area with very fast speed, react rates of this reaction may be determined by the transport of sulphides in the melt to the reaction region. Some amount of oxygen is not reacted and remains in gas region. And the oxygen reacts with SO_2 and SO_3 is formed by Eq.18 when temperature is lower than approximately 600℃ in on-field operating conditions.

$$SO_2 + \frac{1}{2}O_2 = SO_{3(g)} \qquad (18)$$

$$SO_3 + H_2O = H_2SO_{4(g)} \qquad (19)$$

Thus, some of the SO_3 mixed in output gas which is mostly composed of SO_2. This factory moved to sulfuric acid equipment and used to make sulfuric acid. However, it is desirable to remove SO_3 in advance because it can cause problems in the manufacturing equipment of sulfuric acid. To remove SO_3, react with spraying water on the way through the output gas from S-furnace as shown in Fig 19. The mixed gas of SO_2 and SO_3 reacts with water and only SO_3 reacts to make sulfuric acid. (Eq.19) As a result, the water that reacts with the exhaust gas will be acidic and the concentration of this sulfuric acid in this solution is defined as "Weak-acid concentration." Weak-acid concentration is proportional to the amount of oxygen that is not reactive in the furnace, and the amount of oxygen that is not reactive is proportional to the amount of sulfide transferred to the reaction area. And it depends on strong flows which means the ability of mixing in smelting furnace. Therefore, the weak acid concentration could be used as a criterion to judge the ability of the reaction in the furnace. It must be noted that it is important to maintain similar

values of the weak-acid concentration when the process conditions are changed in field operations. Therefore, it is necessary to confirm whether the elevation of the lance causes insufficient mixing for realizing the target amount of reactions. Consequently, we measured the weak-acid concentration for several months to evaluate the effects of the lance height change on mixing. The experimental results (Fig. 20) indicated that the concentration of the weak-acid was nearly equivalent in both the original and modified conditions. This result strongly suggests that the mixing ability pertaining to the lance height of 1.5 m is within the range that does not reduce the ability of the reaction in the present smelting furnace operations.

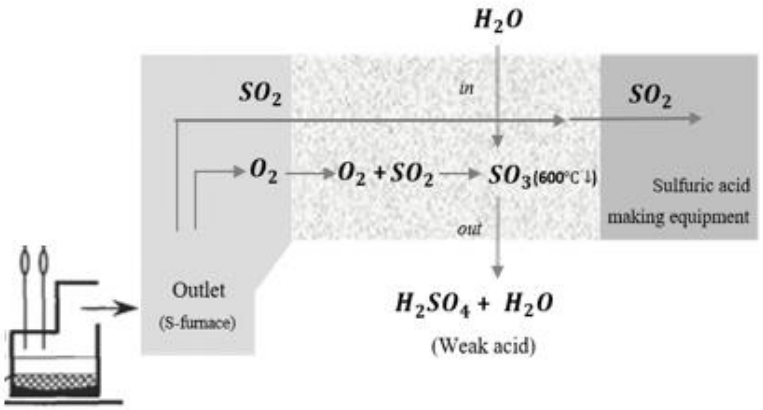

Fig. 19 Schematic of the processes of measuring weak acid

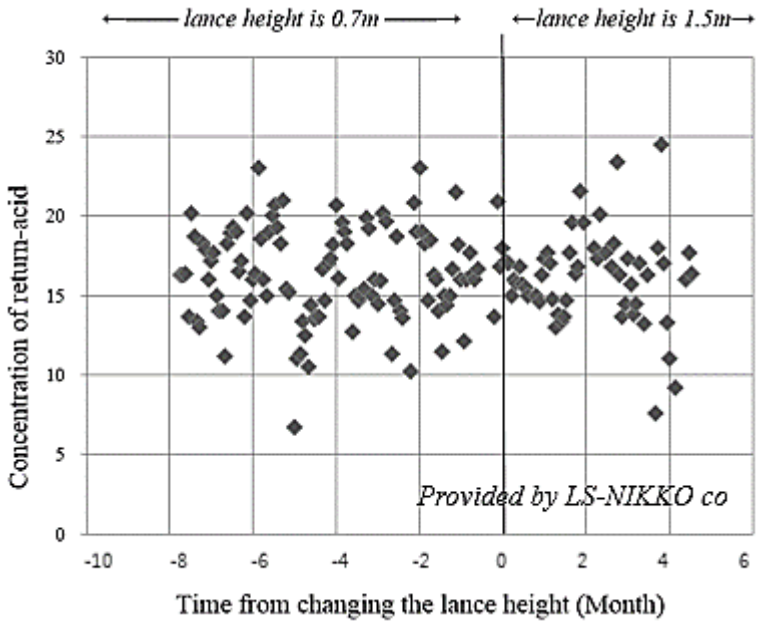

Fig. 20 Trend of return-acid concentration by lance position

3.1.3.3. Remaining hearth brick

Currently, one of the problem is bottom hearth wearing because of injection materials injected high velocity and severe fluid flow. This problem becomes more serious after the number of lance is increased from nine to eleven and the injection of copper concentrate is increased. The experimental results (Fig. 21) indicated that the damage of refractory under the region of lance was decrease.

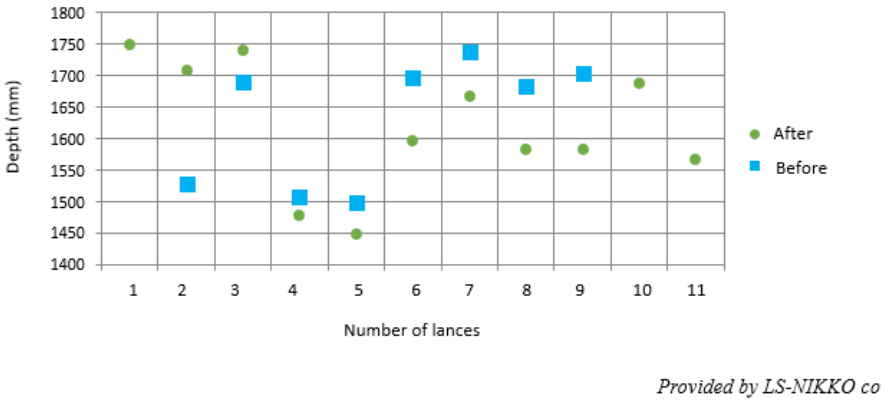

Fig. 21 Trend of remaining depth of hearth brick by lance position

3.1.3 Summary

To study the phenomena in the furnace, we developed numerical analysis models, calculated the transport phenomena using the models, and conducted field experiments. The numerical simulation showed that the lance height considerably influences the transport phenomena in the furnace and suggested that the lance failure could be decreased by raising the position of the lances, as this act could reduce the temperature of the lances. Based on the simulation results, the smelting furnace process was performed with a higher lance position. The number of lances consumed and concentrations of weak-acid were monitored to determine the effects of the change in the lance positions. The results indicated that the number of consumed of lances decreased by approximately 50%, and the concentrations of the weak-acid were nearly equivalent in both the original and modified lance height conditions. Thus, it could be concluded that the use of the modified operating condition could decrease lance failure without the loss of the reaction ability of the smelting furnace.

3.2. Conditions 2: Feeding system

3.2.1 Comparison of feeding system

Current feeding system of S-furnace is batch feeding where the concentrates are fed crossed. In this section, comparison of current batch feeding system with the continuous feeding system that considered to adopt in the future will be discussed. From field data analysis conducted in LS NIKKO. Co, the cycle required for calculation was obtained. As shown in Fig.22, a result of field data analysis, cycle which can be regarded as one cycle could be derived. It took 521 seconds per cycle to fed concentrates across into six concentrate tanks. There are five peaks in a cycle where a lot of concentrates are instantly thrown, and each feed time could be estimated to be about 10 seconds. The positions of lances where the concentrates are actually fed into are shown in the Fig.23. However, there is a physical limitation in applying 521 seconds of flow time in calculation. Thus, transition section(A~J) is calculated and comparative analysis for the inside of the furnace was conducted. With this calculation strategy, it is possible to analyze the area which is not actually calculated when calculation is converged in the areas at the both end, resulting the time required for calculating the whole area can be omitted. Furthermore, from analysis focused on the transition sections where show significant difference with continuous feeding, it can be expected to understand the phenomenon in the furnace caused by batch feeding. Areas were divided into 5 steps A to E in chronological order based on the transition section where peak appears and each area is subdivided into 3 parts according to the positions and the number of lances which concentrates are fed. (Fig.24) Based on the assumption that the

amount of concentrates fed per unit time through each lance is equal, the total amount of injection is derived for each part, and numerical analysis is performed using this value.

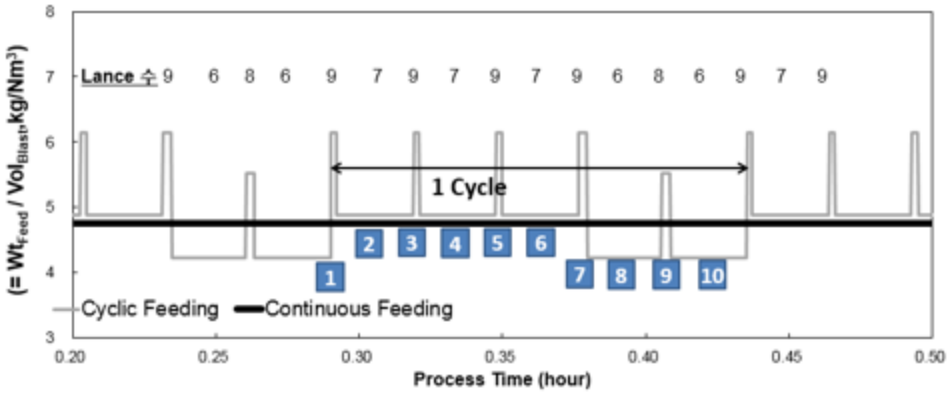

Fig. 22 Time-Based relative amount of injection (1cycle)

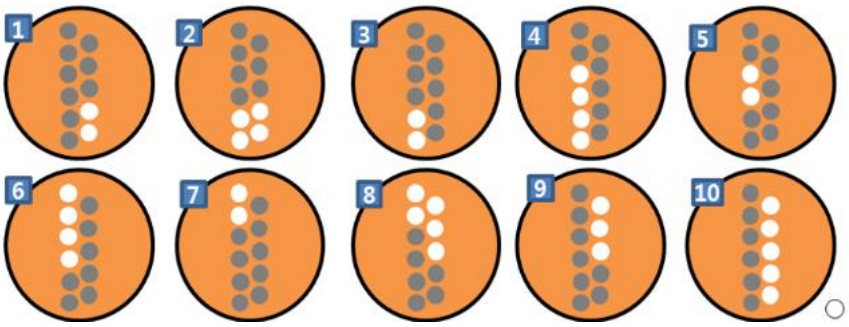

Fig. 23 Lance location where concentrates are injected (●)

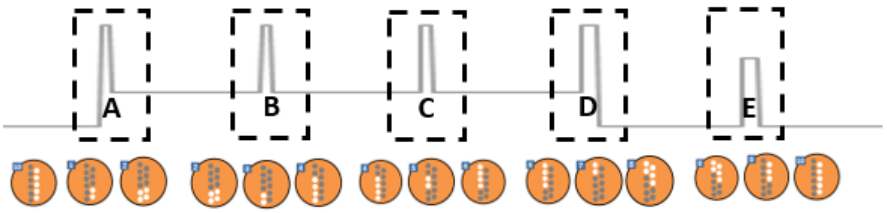

Fig. 24 Step A-E based on computational strategies

3.2.2. Result of computational analysis: Melt velocity

a. Continuous Feeding

In the case of continuous feeding, the calculation was conducted under the assumption that the 11 lances continuously inject a certain amount of concentrates (4.8 kg/s per lance). Since there is no change in the injection condition, the speed in the matte becomes relatively constant after the calculation time proceeds (the convergence state is reached). If continuous feeding operation is performed in the field, the injection flow time will be significantly longer than the flow time calculated by CFD. Consequently, the area determined to be converged under the present condition can be understood as the area can be predicted in actual operation. Melt velocity with respect to time in the 'post-convergence section' is shown in Fig. 25. As this model has severe turbulence, strong fluctuation occurs. For this reason, we try to calculate and compare the average value of time, which is 84mm/s.

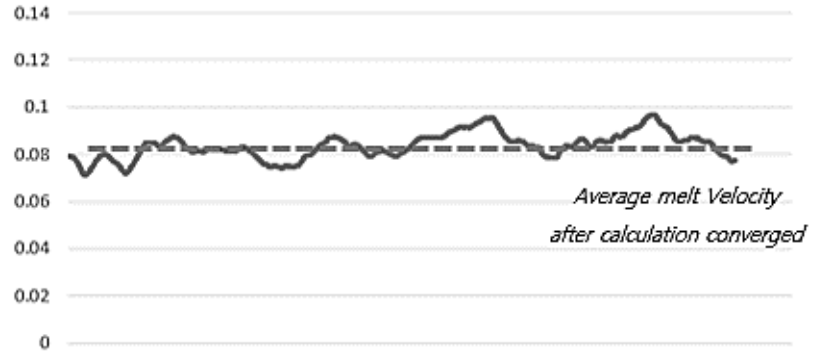

Fig. 25 Average velocity of melt in continuous feeding

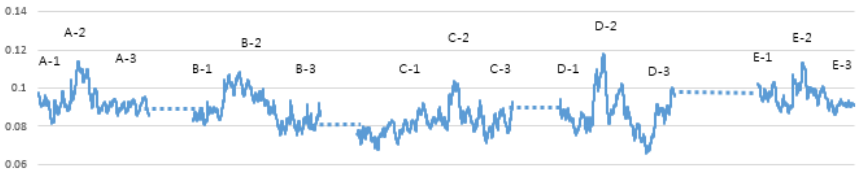

Fig. 26 Batch feeding melt average velocity in all areas

b. Batch Feeding

In the case of batch feeding, unlike continuous feeding, the conditions vary according to time. There are three conditions for each step, and the change at the peak in the center that concentrates enters from 9 lances are calculated for 10 seconds and for both edges calculation proceeded until it is converged.(Calculation time varies in part by condition)

After the calculations for each part were made individually with batch feeding, the results of melt average velocity in all areas were organized in chronological order (Fig. 26). In all areas, there is a fusion induced by warm current, and the second part of each step, which is particularly heavily charged, shows a strong flow (a-2, b-2, c-2, d-2, e-2). This is because the flow rate in the furnace is generated from the momentum of the material to be charged, so the average flow rate generated as the amount of concentrates to be charged increases. The average result value for each part is derived from the results and summarized in the Fig.27. In addition, the average value for each area is taken as a result for the entire time and the actual flow time (521 seconds) of the batch feeding cycle. As a result of calculating melt average velocity in the value is 92 mm/s. Melt average velocity values in continuous feeding and batch feeding are 84mm/s and 92mm/s, respectively. The average flow rate is a little lower than that of batch feeding, which is thought to be relatively stable injection condition is maintained continuously.

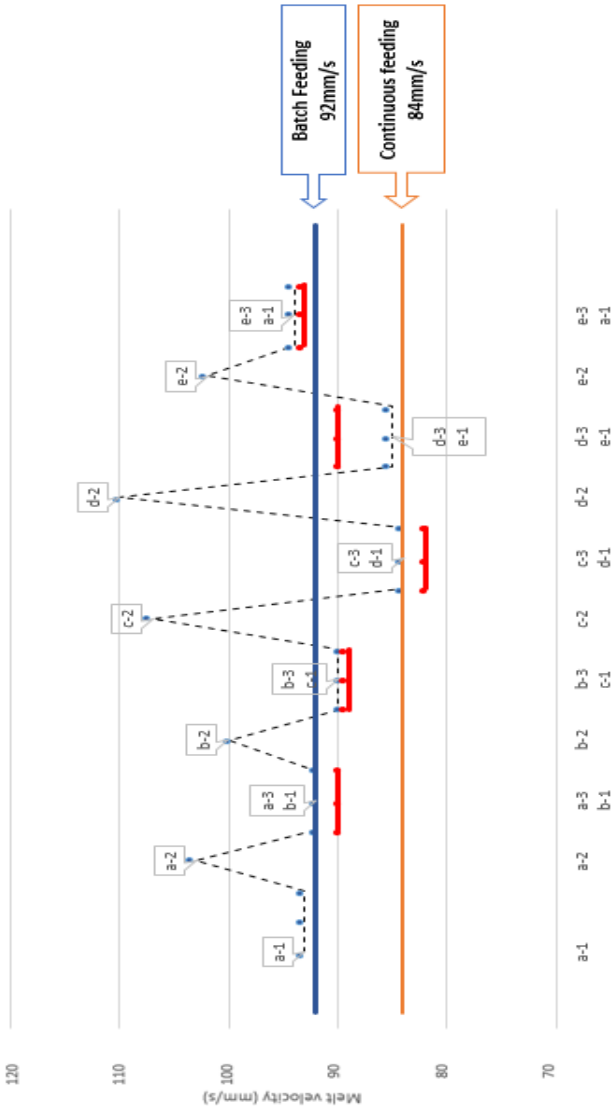

Fig. 27 Melt average velocity with batch feeding and continuous feeding

3.2.3. Result of computational analysis: Penetration depth

Penetration depth means the depth generated by the concentrates and gas injected through lance from the melt surface. Although the depth itself has no significant physical significance, it can be used as a reference for verification of the calculation result and for comparison of other changes in the magnitude of lance momentum since it has an experimentally presented value.

The definition of penetration depth in this subject is the depth of melt produced by the injected material. However, quantitative figures are not provided to indicate the depth or percentage of a specific substance. In the current CFD, criteria are required to analyze penetration depth, and we defined and compared the depth range from one point to the zero end of the air under the matte surface (Melt volume fraction=1 to 0) penetration depth. (Fig. 28) The penetration depth defined within the range can be selected depending on the analysis to be performed. However, considering the MI equation experiment method, it is appropriate to compare the maximum depth of this. Thus, subsequent penetration depth compares the maximum depth value (Air volume fraction=1) that can be occurred at a specific position.

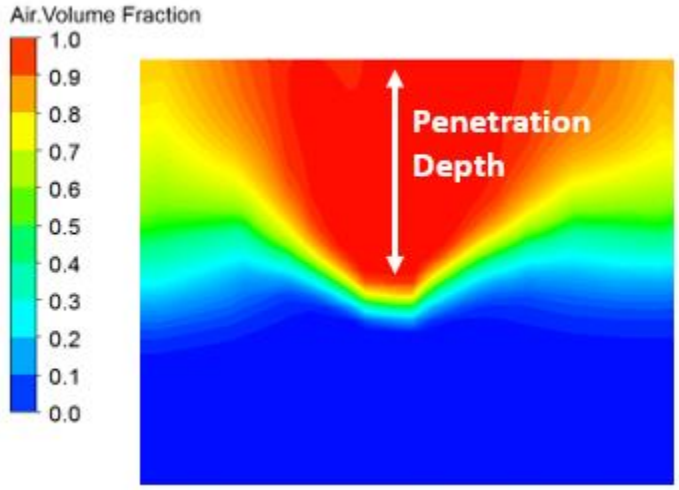

Fig. 28 Penetration depth in CFD

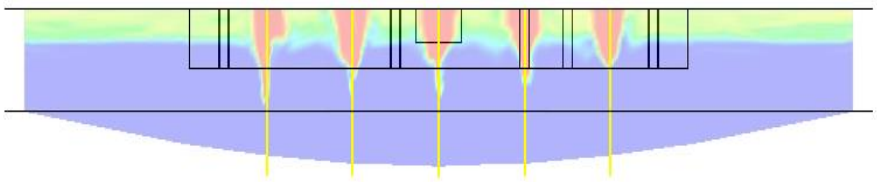

Fig. 29 Penetration depth result derivation location

Fig. 29 shows the location and method of deriving penetration depth data. A line is generated perpendicular to the center of each lance, and the penetration depth result is calculated by reading the coordinate value for the highest point of a number of cells where the volume fraction of air is 1 in the region where the melt exists. In the case of penetration depth, the variation in the flow rate of the low internal melt is large. Thus, there must be a change in the value depending on the time. This is because in multiphase flow, the two phases (Melt, Air) interact continuously along the interface with each other, and the air thrown in is directly affected by the movement of melt, which already has a severe flow. Comparing the two feeding systems, batch feeding has a deeper penetration depth value than continuous feeding. In the case of judging on the basis of one lance, the other conditions are the same and the amount of concentrates charged is different from 7.6 kg/s and 4.8 kg/s, so that the penetration depth generated in the furnace is different. CFD calculation results vary with time and therefore mean the overall results should be derived. As a result of average data, batch feeding penetration depth is 110 cm on average and continuous feeding is 89 cm on average. The result of calculation by MI equation is 93 cm and 70 cm respectively. (Fig. 30) The trend is similar to the calculation and theoretical equation, but the values are slightly different. There are several possibilities for these differences to be sent.

First of all, there may be difference because the experiment was conducted on a model. In addition, it is possible that the calculated cavity formation was calculated in excess of the experiment. Another possibility is that the value measured in the experiment is not in the center of the region but in the periphery.

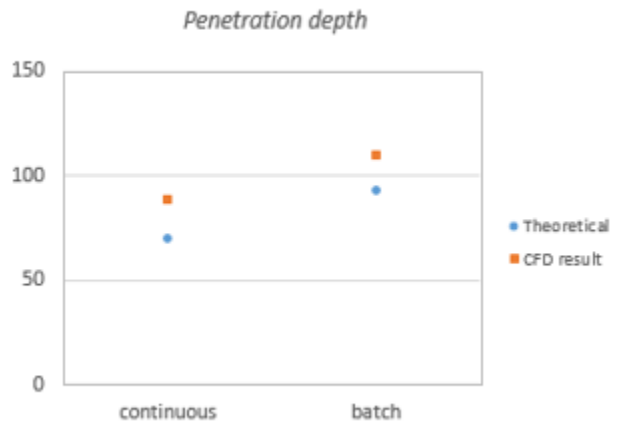

Fig. 30 Penetration depth comparison (MI equation vs CFD result)

3.2.4. Result of computational analysis: Melt splash

In the calculation, the amount of melt splashed into the atmosphere in the furnace is calculated by the VOF model. In field operation, splashed melt exist discontinuously in a continuously existing gaseous state. However, the VOF model is a method for advancing calculation on the assumption that images to be calculated continuously exist at each position in the calculation area with a specific volume fraction. In the calculation, when the amount of splashed particles under different operating conditions is compared, the fraction of the particles is 0.1 (volume fraction) or more in the region and used to reduce difference. (Fig. 31) The amount of splashed melt is also calculated in continuous feeding, averaged amount of melt in air is 38.7m^3 and 50.2 m^3 in batch feeding.

From results, it can be found that the amount of splash is 30% higher at batch feeding system. Assuming that the amount of injection material is similar, this value is quite high. The biggest reason for this increasing is that splashed particles do not immediately return to melt under the condition that materials are injected continuously, but float for a period of time in the gas region.

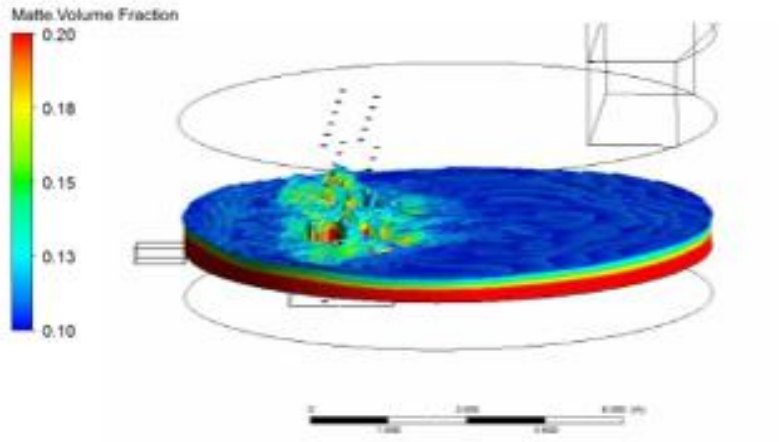

Fig. 31 Melt splash in air region (Melt volume fraction≥0.1)

3.2.5. Result of computational analysis: Reaction area

The average speed of the melt is used as an important factor for displaying the reaction rate in the field. The Mitsubishi process estimates that the particles contact with the melt are absorbed by the melt before the particles react, in order to inject the particles of low temperature into the melt at a high speed, and estimates that the chemical reaction occurs when the oxygen comes into contact with the melt. If the rate determining step to the reaction rate is considered as dominant, and the rate determining step to the reaction rate is considered to be reasonable to some extent, when the new melt is transmitted to the reaction position in the melt region.

We found that the behavior of cavities at the bottom of the lance was very different when particles + gas and gas were injected. As explained in detail in 4.2.1-4.2.3 below, the gas/melt interface area is larger when the gas/melt interface area is continuous in the cavity where the reaction is expected, meaning that batch and continuous reactivity are different. If the reaction area maintains a similar value, the reaction degree can be deduced with a melt tempo, but if the reaction area changes, the validity of predicting the reaction degree can be limited.

In particular, no cavity is formed at the bottom of the lance where no concentrates are charged together in the batch, which means that the rate of reaction of the injected oxygen with splashed particles or gases is higher than that of meeting and reacting with melt. In this section, the work of analyzing the effect of this difference on the reaction tendency and the degree of reaction is not progressing, and the effect of such a change in gas/melt reaction area on

smelting reaction is expected to be a very important variable for understanding and improvement of the phenomenon that will occur when continuous operation is implemented. In continuous feeding and batch feeding, we confirmed that there are differences in the form and degree of gas being put into melt depending on the injection conditions. In the case of batch feeding, the results of this study were compared to each other on condition that the same amount of concentrates as the continuous feeding (approximately 50 kg/s) would be contained due to various cases.

a. Continuous Feeding

In continuous feeding, all lances emit the same amount of concentrates and gas. Although the air volume fraction form directly under each lance is different due to turbulence, the formation of penetration depth is approximately the same. (Fig. 32) To calculate quantitatively, as a result of drawing a graph about the degree to which the air phase exists at the position of each lance center circle, all the results can confirm that gas is fed to a specific region through the surface of the lance. At this point, the maximum depth is penetration depth. (Fig. 33)

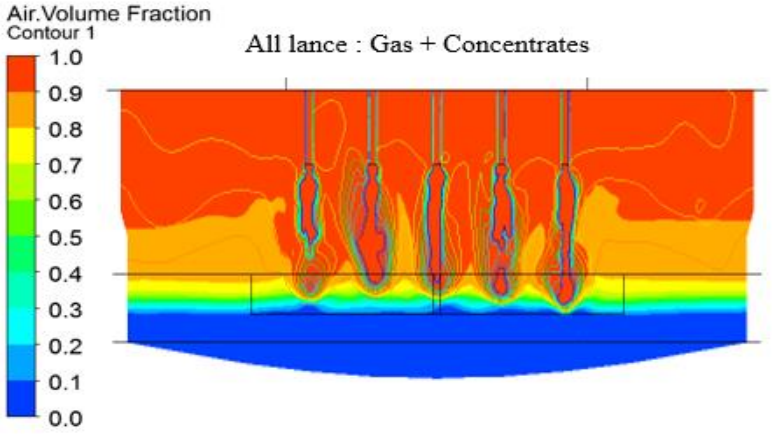

Fig. 32 Air volume fraction contour in continuous feeding

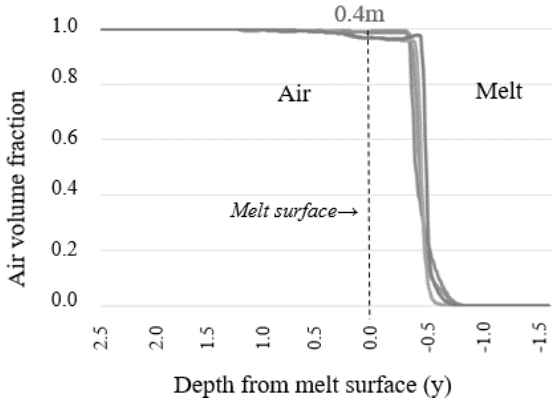

Fig. 33 Air Volume Fraction in Continuous Feeding

b. Batch Feeding

In batch feeding, gas is injected in all lances, but concentrates are injected from a specific lance by time. The gas injected with the concentrates reaches the surface of the melt to form penetration depth, but if only the gas comes out, it can be confirmed through Fig. 34 that it does not reach the melt completely. This determines that when splashed melts are mixed in the air area during operation and only gas comes out through the lance, there is insufficient energy to reach the surface of melt through the splashed melt.

We have quantitatively drawn and confirmed the degree of existence of the air phase at the position of each lance center circle in the same way as the continuous feeding (Fig. 35), and as a result, we can see that the amount of gas reaching the surface of melt is very small in the area under the lance. The common reaction in which gas reacts internally with melt and oxygen in a lance where only gas can be joined may be used in other forms of secondary reaction (where only gas can enter some lances, such as batch feeding). For example, there is a high possibility that the reaction between melt and gas that splashes to the mountain instead of inside melt (reaction position change), and the reaction between SO2 and injection gas generated after the main reaction are more active than expected.

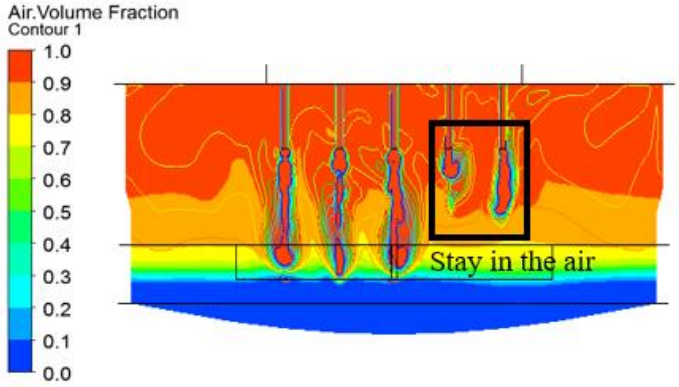

Fig. 34 Air volume fraction contour in batch feeding

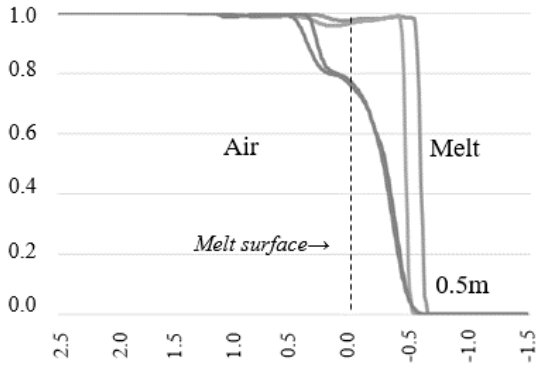

Fig. 35 Air volume fraction in batch feeding

Determining whether such behavior is advantageous or disadvantageous to S–furnace in the current situation is tricky. In particular, the current operation result is based on this behavior because the injection pattern of the batch type is currently operated. Thus, if the injection pattern is changed to continuous type, it is expected that the change in the reaction region obtained in this study will give a lot of suggestions on the interpretation of the effect on the preparation of matte and improving the process of the operation conditions.

In order to understand the differences between the above forms of penetration, the reaction inside the melt in theory should be discussed first.

There are two preconditions in S-furnace. The concentrates melt as soon as they arrive at the surface of melt because the melting point of the concentrates are 680°C, and melt maintains about 1240°C. Second, the kinetic results in the theoretical analysis show that melt reacts with oxygen in 10 ^(-1) ms. This can be regarded as instant reaction occurs in the current process. Based on the above two assumptions, main reaction is an FeS oxidation, and the reaction position is the interface between rising bubble and molten melt. (Fig. 36)

$$\mathrm{FeS\ (l)} + \frac{3}{2}\mathrm{O_2} = \mathrm{FeO\ (l)} + \mathrm{SO_2} \quad (20)$$

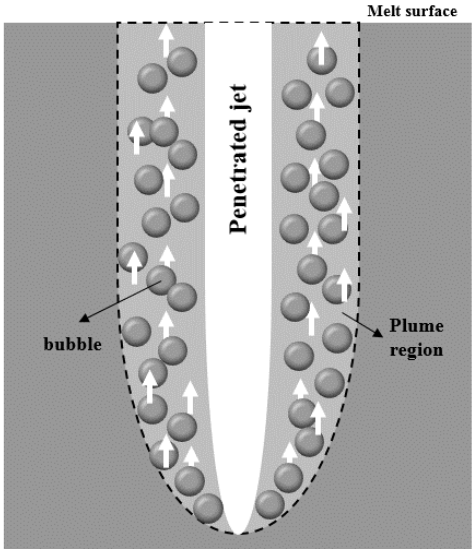

Fig. 36 Main reaction mechanism in smelting furnace

The mechanism for this reaction is as follows. First, oxygen is jetted from a lance, and while forming a cavity on the surface of the melt, it meets the melt on the surface of the cavity. As FeS is eliminated by the reaction on the cavity surface, it must be moved to the cavity surface inside the melt toward a new reaction. As a result, oxygen and FeS meet and react on the cavity surface. Since a thin boundary film between liquid and gas is theoretically formed near the surface in this reaction process, there are three mechanisms in the surface region.: Transmission of FeS by liquid film, Transmission of oxygen by interface film, and Chemical reaction) Actual reactions require the transfer of generated substances, namely, the transfer of FeO into the melt and the transfer of SO2 into the atmosphere. However, this mechanism is symmetrical with the movement of reactants, so there is no need to consider it separately. The reaction rate is determined by the slowest of these five mechanisms, which is called rate determining step, and the variable associated with this mechanism is changed to improve the reaction rate. The bubble was formed near the interface where the three mechanisms exist, and it seems that they are proceeding at a rapid pace.

Melt bubble occurs because heavy flow near the surface of the cavity due to the injection materials being thrown into the melt, it causes instability of the interface. The bubble, thus formed, should be moving like shown in Fig. 36 to create an increasing in the transmission rate of o2 and FeS and an increasing a the reaction area, and the three mechanisms that exist near the interface should be faster.

Further, since oxygen is jetted from a lance at a very high speed, it is transmitted very quickly. Thus, it is expected that the mechanism through which reactants are transmitted to the interface within the melt determines the reaction rate. Because the transfer of material to the interface inside the melt is determined by the flow velocity and turbulence of the melt, it is reasonable to consider that the current melt flow velocity is an important factor for reactivity.

However, the reaction area is not covered. The above approach is basically analyzed in a similar situation, and the reaction tendency of both systems will change greatly if the reaction area changes.

In comparing the reaction area when the method of supplying concentrates changes from batch to continuous, the reaction area increases significantly as explained in below. Also, if the reaction area of the batch is small, it is necessary to confirm the behavior of oxygen jetted from a lance having no cavity formed. For this work, we examined the velocity distribution of gas and melt in detail.

In the case of continuous feeding on the lower stage, cavities are formed under all lances, and the vectors generated at that time are in the form of vectors as shown in Fig. 36. In the case of continuous feeding, the amount of concentrates charged per second is 4.8 kg less than that of batch feeding, and the charged gas is transmitted to the melt under all lances even though the depth of the penetration depth is relatively shallow. (Fig. 37)

On the other hand, batch feeding has two cavity shapes. Thus, it is necessary to understand the behavior of the gas in the melt in each case. First, we confirmed the behavior of gas under a lance in which gas and ore are

simultaneously charged. In this case, the condition that contributes to the reaction when the bottom injection material of the lance reaches the inside of the melt and enters, that is, the bath smelting is satisfied. (Fig. 38) When only the gas is charged as in Fig. 39, the gas was not completely in contact with the melt surface. The cavities were also not formed and the injection gas was allowed to move only on air, which offers the possibility to have other reaction forms, secondary reactions, rather than bath smelting.

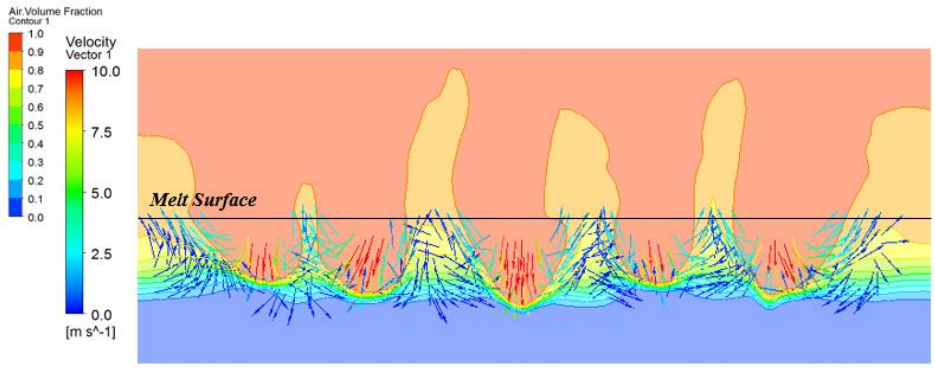

Fig. 37 Gas behavior in melt in continuous feeding

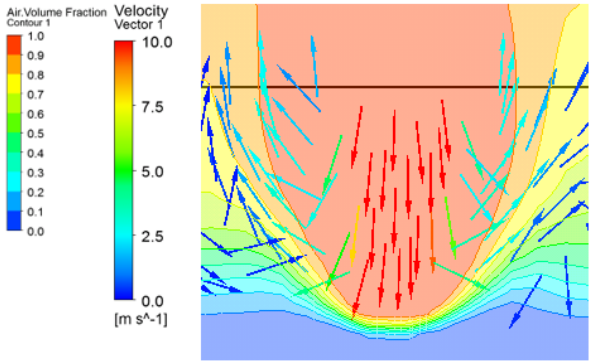

Fig. 38 Batch feeding gas behavior in melt - under lance the concentrates and gas injected

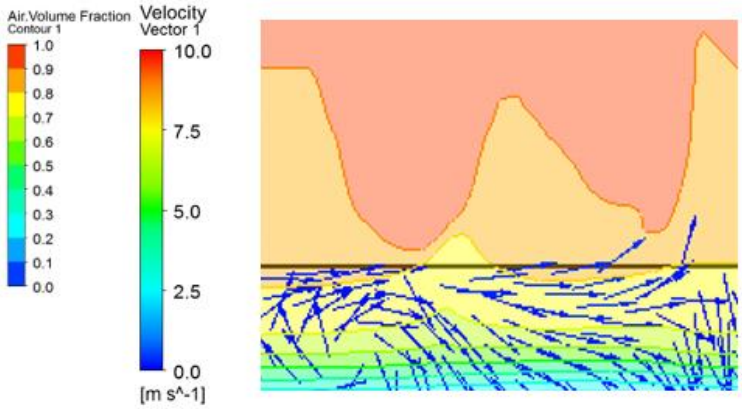

Fig. 39 Batch feeding gas behavior in melt - Under lance the gas injected

Data of the reaction region were derived by CFD calculation for relative comparison of reactivity. First, we derived the area where the volume fraction of the air in melt is 1 among the depth ranges compared as penetration depth and compared the surface area. Since the reaction in the furnace is an interfacial reaction, the area of the volume of penetration depth is analyzed. The amount of ore that enters is similar in both batch and continuous feeding. But the surface area generated during continuous feeding is 10.6m^2, and 7.8m^2 for batch feeding. (Fig.40-41)

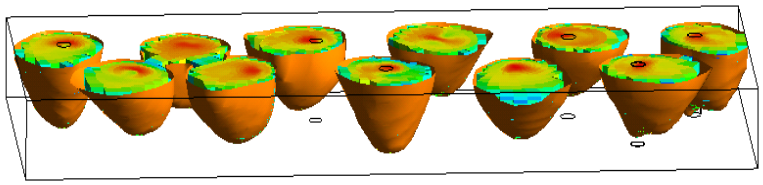

Fig. 40 Reaction area in continuous feeding

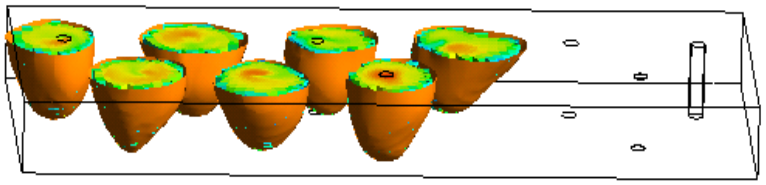

Fig. 41 Reaction area in batch feeding

Since this area varies with changes in the amount of concentrates entering and flow, the value was derived from the entire batch feeding cycle (Fig.42) the average value were compared. In the case of continuous feeding, the average area size is 11 m^2, while in the case of batch feeding, it is 7m^2 when the total time is averaged. In general, continuous feeding is advantageous from the reaction side because the reaction quantity increases as the reaction area increases. However, if there are many parts that react with splashed particles from a lance that injects only gas through batch feeding, the reaction area can be increased, so it is possible to make a quantitative decision only with an in-depth analysis.

However, it is clear that the reaction form of continuous injection is different from the batch type, and it is expected to be a more suitable reaction type to implement the smelting reaction pursued in the Mitsubishi refining reactor.

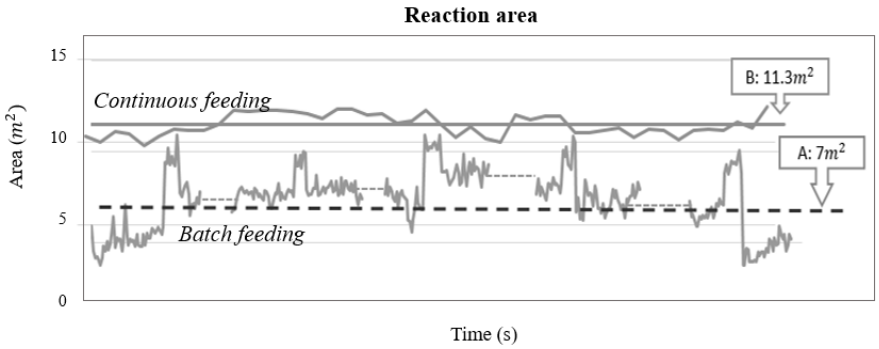

Fig. 42 Change of reaction area and average values by feeding system

3.2.6. Result of computational analysis: Temperature of lances

From comparison of continuous feeding with batch feeding system, the internal flow was affected by whether concentrates were continuously fed through lances or crossed through the lance. However, it was examined whether there was a difference between the feeding system as well as the flow in the furnace depending on the feeding system.

Figure 43 (a) and (b) show the total temperature distribution of the lances in each feeding system. Figure 43 (a) shows the temperature of 11 lances in continuous feeding. The temperature of lance is lower than that of the surrounding environment because concentrates is continuously injected through lance. On the other hand, in the total temperature distribution of the lances in batch feeding (Fig. 43 (b)), the temperature of lances containing gas only (four right lances in Fig. 43(b)) were relatively higher than that of lance containing concentrates (seven left lances in Fig. 43(b)). This can be understood as the influence of the amount of heat that the material injected into the lance took from the lance, namely, the difference due to the heat capacity of the injection material.

Inside the furnace, a high temperature atmosphere of 1,200°C or more is formed due to heat of reaction. However, the material injected into the lance is initially at room temperature and the temperature rises as it passes through the lance. Instead, the temperature of the lance itself decreases and the degree depends on the types of feeding materials.

From the results, continuous feeding will maintain a certain level of temperature under the same feeding condition. On the other hand, in the case of batch feeding, it is expected that the material injected to the lance will change with cycle and will change the temperature of the lance will change continuously.

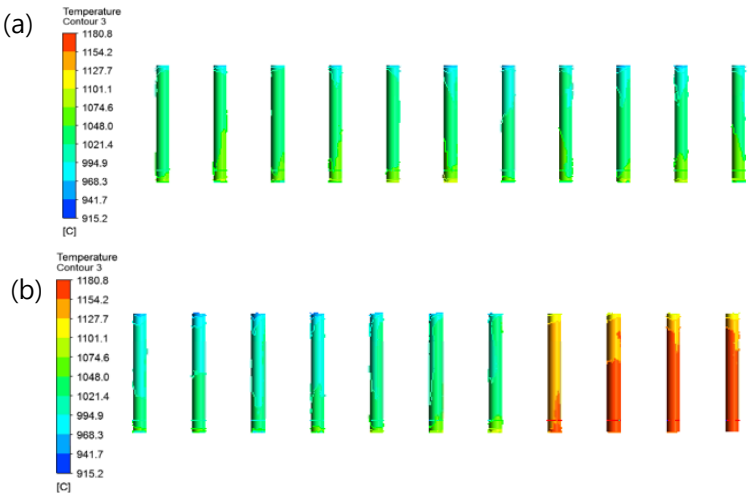

Fig. 43 Lance temperature distribution in (a) continuous feeding (b) Batch feeding

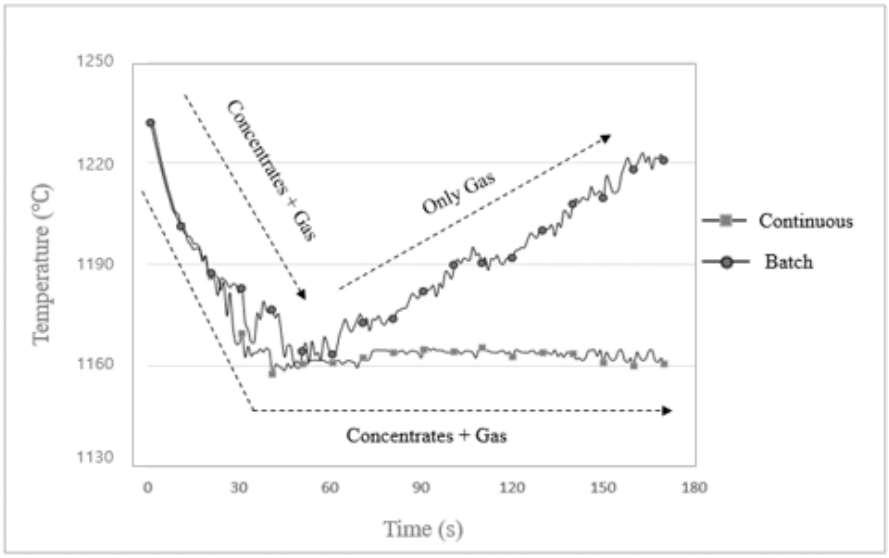

Fig. 44 Variation of temperature by feeding system

Chapter 4. Results of Microstructure analysis

The lance into which concentrates and oxygen are injected is broken randomly in the furnace, but no clear reason for this has yet been revealed. We're trying to analyze how the material side of Lance Street has affected us through specimen analysis. The test piece was actually used as S in LS-NIKKO during the process. Experiments using both unused lance and used lances were conducted. Used lances means that the lance was used in field operation. Samples were taken from lances, which were made of high-chromium stainless steel [11]. We numbered the samples according to the experimental conditions.

Sample 1 is taken from new lance before used in process. Sample 2 was taken from a tip of remaining part of fractured lance. Sample 3-1~3-7 were obtained from a used lance which was drawn before fracture had occurred. Especially, in the case of sample 3, 7 samples were taken from different positions of the lance. Sample 3-1 located at the tip of lance and other samples were taken 10cm above sequentially. So sample 3-1 was located at the lowest position and sample 3-7 was located at the highest position and 60cm above sample 3-1.

Sample number	Specimens were taken from	Experimental conditions	Experimental environment
1	Unused lance		
2	Used lance	Tip of remaining part of fractured lance	Field experiments
3	Used lance	Drawn before occurrence of fracture and samples are taken 7 different positions of lance, 3-1~3-7	Field experiments
4	Unused lance	Reaction to lance and matte at different temperatures, 4-1(1100°C) and 4-2(1090°C)	Lab experiments

Table 4 Samples used in the present study

Laboratory experiments were also conducted. Three samples were taken from unused lance and powders of matte from smelting furnace of a company were collected. The matte powder was placed on crucibles. The exterior of the lance sample was put on top of the matte and placed facing the crucible bottom for the continuous supply of matte. Hydrogen gas was injected to avoid of the other reactions and the crucibles were kept at a temperature for 8 hours in 1100 °C (sample 4-1) and 1090 °C (sample 4-2) respectively. All of experimented specimen were analyzed to figure out the reaction behavior of lances. In order to analyze the results of reaction, the outside of lance, which is directly affected by the environment of smelting furnace, was mainly observed. we called this part as exterior and another side as interior in specimen. Scanning electron microscopy (SEM) and energy-dispersive X-ray spectroscopy (EDS) analyses were used to observe the morphology and compositions. Additionally, the electron backscatter diffraction (EBSD) analysis was conducted to observing the phases of the fracture lance. A thermodynamics program (Fact-Sage 7.3) was used to calculate the phases of the lance, and the reaction of the lance with matte during operations.

4.1. Unused lance and used lance

Since the lance currently used is a product that is arbitrarily cast and used due to its forgery, it is necessary to analyze the lance which is not used. Analysis of the image (Phase) and decision direction through EBSD. (Fig. 46) The pre-use lance was confirmed to be duplex stainless steel, which was a mixture of BCC ferrite and FCC Austenite. EDS quantitative analysis mapping image analysis results of lance before use are as shown below. (Fig. 45) The following analysis results confirm that Cr and Fe carbide are formed along the entrance. In the case of chromium, less is found in the austenite region around the grain boundary than in the mouth. This can be deduced that Cr has been volatilized by the formation of carbides in grain boundaries. Based on the analysis results, the difference in thermal expansion coefficient between FCC austenite and BCC ferrite may accumulate due to lance residual thermal stress when the temperature change of the lance is high. Further, it can be confirmed that Cr is volatilized by forming the carbide along the entrance of the field in a high relation of the content of C. As a result, there is a possibility that there will be a change in the phase around grain boundaries. The following is a sample EBSD analysis of the broken lance after a high temperature operating environment. (Fig. 47) The outside surface of Lance is FCC Austenite, and the lance body is a mixture of austenite and ferrite. The two percentages differ from each other in measurement of lance and broken lance prior to use.

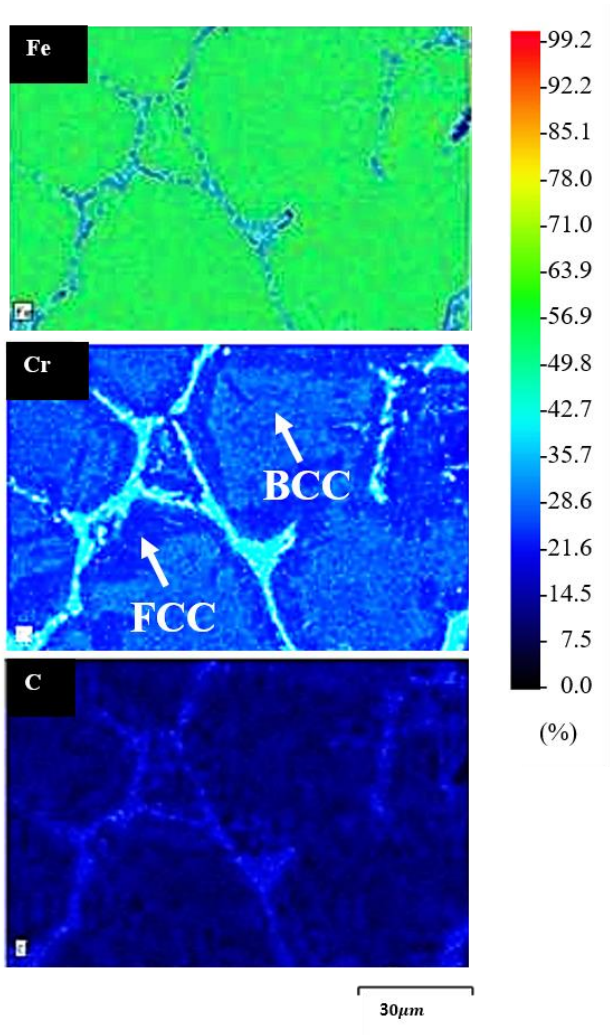

Fig. 45 EDS quantitative mapping of unused lance for C, Fe, and Cr

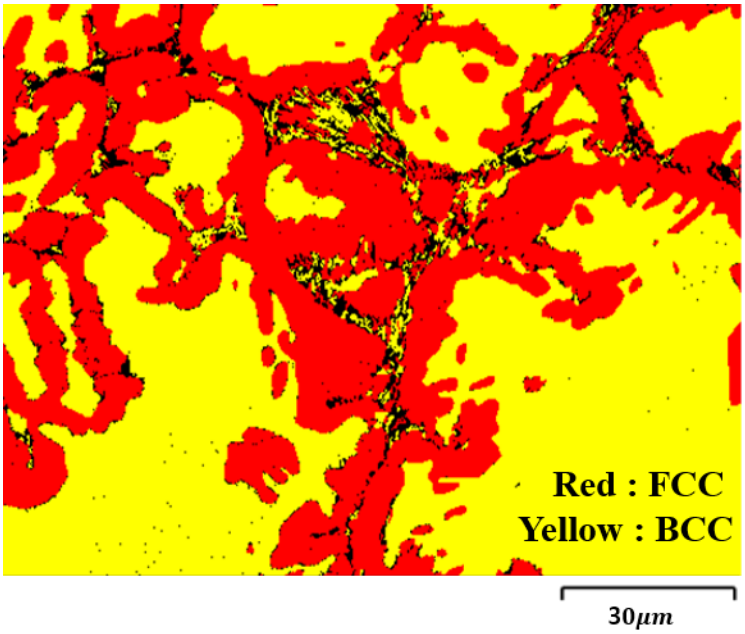

Fig. 46 EBSD analysis results of the unused lance.

The concentration profile of the used lance exterior mapped by quantitative EDS are shown in Fig. 48. The images show that Cr was depleted on the surface because of the Cr depletion, the BCC phases with high Cr in this region might be disappeared. The phenomena of Cr depletion could be caused by the evaporation phenomenon of Cr, which is common in stainless steel. [11] Cr depletion was observed from the microstructure of the fractured lance with EDS analysis shown in Fig. 48. Based on this kind of Cr depletion experiments, it can be insisted that Cr evaporation might be the main cause of material performance degradation. [12] However, the above results are based on the investigation of the remaining part of lance which located upper region of the position where fracture occurred. Therefore, it is not clear that this Cr depletion might be main mechanism of the lance fracture of smelting furnace. Fig.48 also shows that elements such as Cu, O and S penetrated to the lance along the damaged grain and these elements should come from matte (sulfides) or slag (oxides). This shows that matte and slag could be splashed and attached to lance. S reaction can be appeared between the attached matte and lance materials.

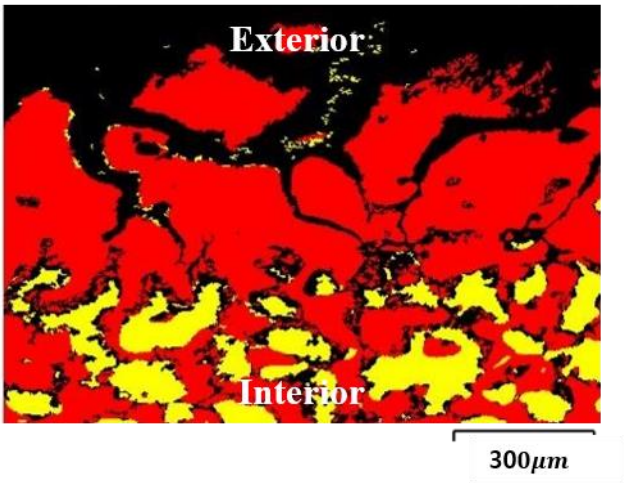

Fig. 47 Results of EBSD analysis.

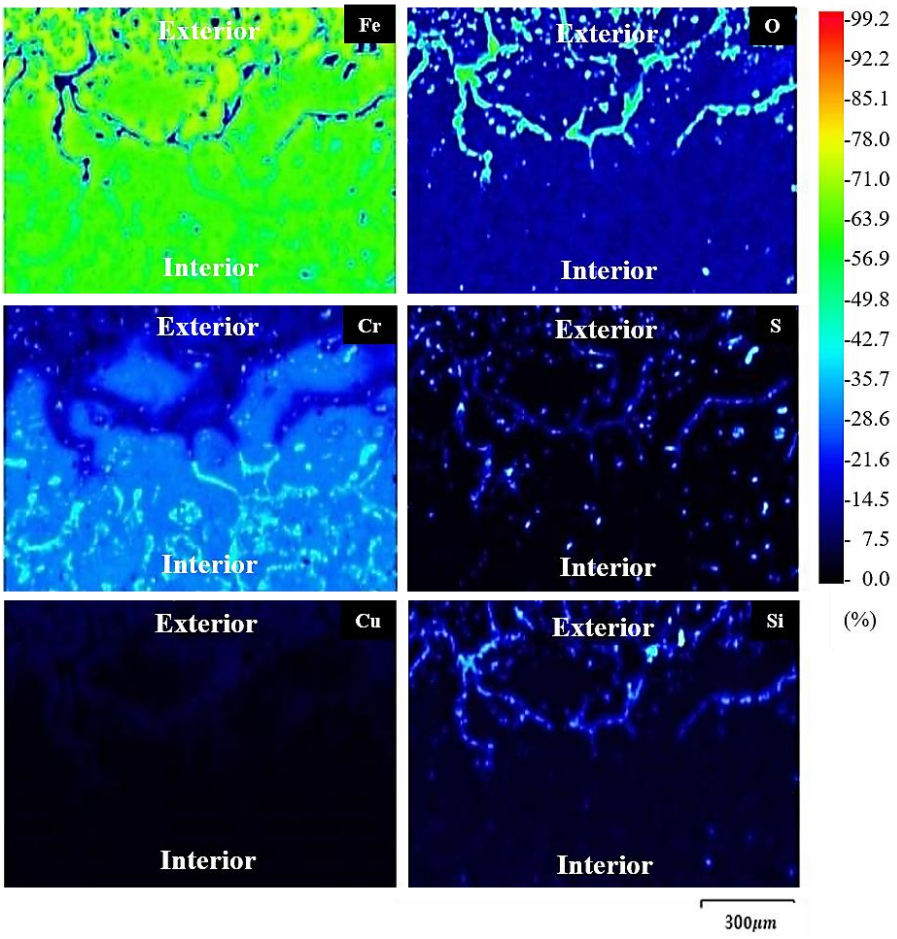

Fig. 48 EDS quantitative mapping near the exterior surface of the fractured lance for Fe, O, Cr, S, Cu and Si

The following is the result of AES analysis. (Fig.49-50) The experimental sample measured the part close to the lance body. As a result of analyzing the wave cross section, it is difficult to clearly distinguish between the two reasons why Lance breaks because inter-granular and trans-granular features are mixed.

As a result of measuring the grain boundary part, Cr is present in most grain boundaries together with Fe and C, and S is present together with Mn and Cr. The presence of Cr in the ingress and partial MnS in the ingress matches the EDS mapping result. However, in order to know exactly what composition Cr exists, a deeper study needs to be carried out with high-performance equipment.

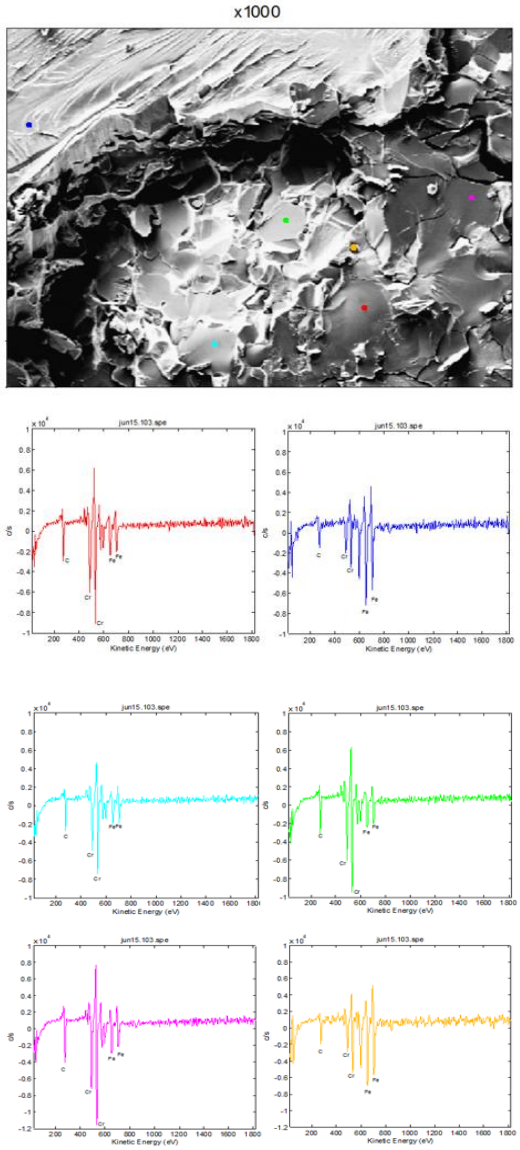

Fig. 49 AES Results for fractured lance (1)

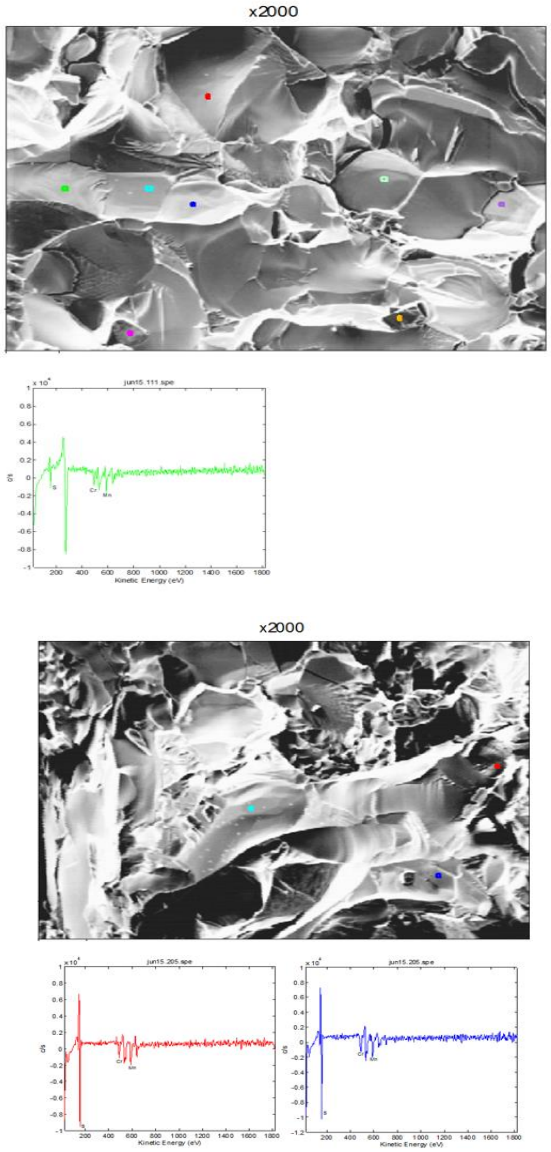

Fig. 50 AES Results for fractured lance (2)

Lance is a duplex stainless steel containing high Cr. In the case of this composition, the resistance to thermal fatigue is good, but the resistance to corrosion of lances is weakened by the atmosphere of high temperature and high sulfuric acid in the furnace. The exact cause of Cr volatilization is unknown, but splashed of matte and slag can affect Cr volatilization. Further, S, Si and O also affect the weakening of cracks on the lance surface by segregation and infiltration of grain boundaries. Repeated cycles of 800 degrees and 1300 degrees under weak lance surfaces can cause thermal fatigue. This can be determined as the cause of the crack in the lance and can result in the propagation of the crack inside the lance by the sustained thermal stress, and finally the rupture of the lance. For this reason, it is judged that a material having high resistance to thermal fatigue should be used. If the range of the temperature change of the lance is more stable than the conditions under which Cr is volatilized, the breaking problem of the lance may be reduced.

4.2. Used lance in various height

To determine the main cause of lance fracture, a lance was drawn before fracture occurred and the lower part of it was analyzed. Samples 3-1-3-7 were obtained from the used lance. The vertical positions of the samples were different from each other. Therefore, the temperatures that the samples were exposed to were different for each samples. Numerical simulation results showed that the temperature of the lance tip was highest and decreased as the position in the lance increased [22]. Therefore, the 3-1 sample was exposed to the highest temperature and the 3-7 sample was exposed to the lowest temperature among the samples. Fig. 51 shows the image of SEM for the 7 samples which exhibit surface damage. The exterior parts of samples were deeply damaged in from sample 3-1 to 3-5 but sample 3-6 and 3-7 were relatively less damaged. To quantify the extent of the damage, the depth of damage was measured on each sample. Fig. 52-27 show the image of SEM and EDS quantitative mapping near the exterior surface from sample 3-1 to 3-7.

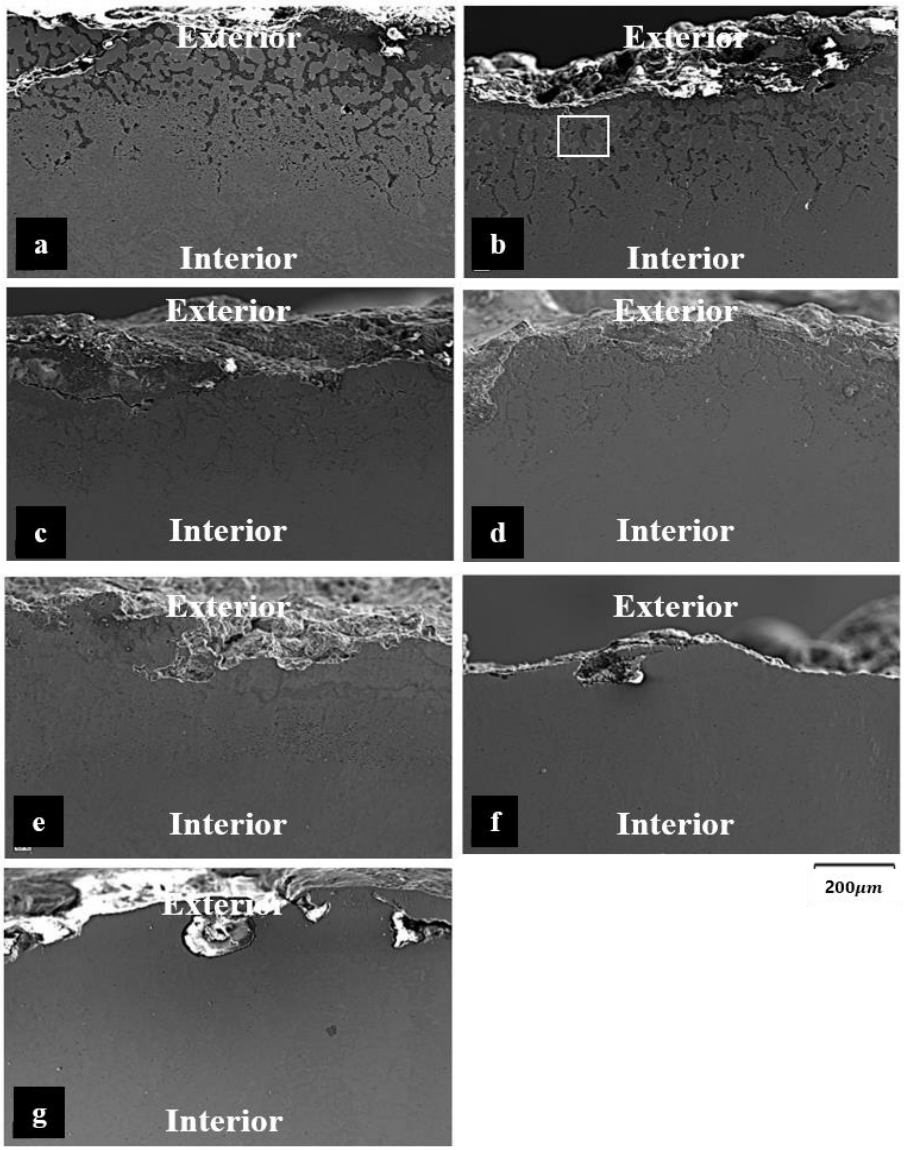

Fig. 51 SEM image of (a–g) Sample 3-1~3-7, respectively.

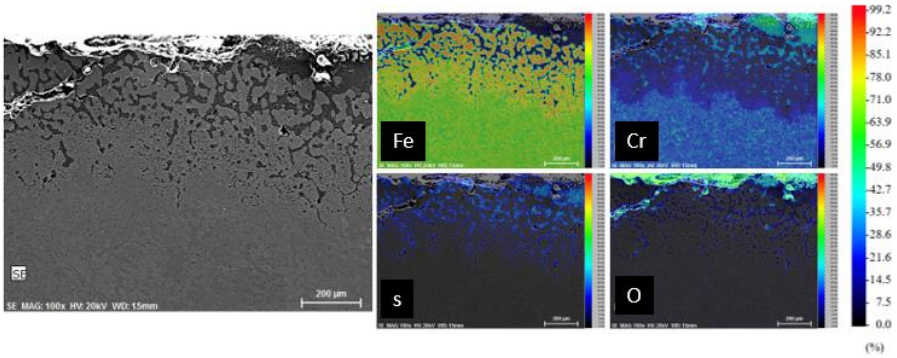

Fig. 52 Image of SEM and EDS quantitative mapping near the exterior surface (Sample 3-1)

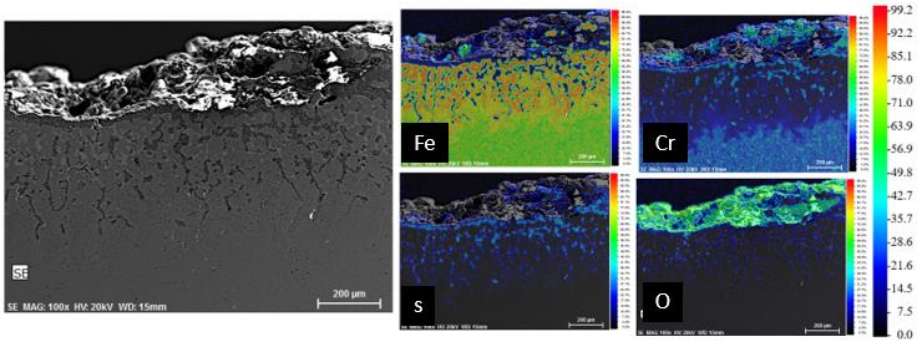

Fig. 53 Image of SEM and EDS quantitative mapping near the exterior surface (Sample 3-2)

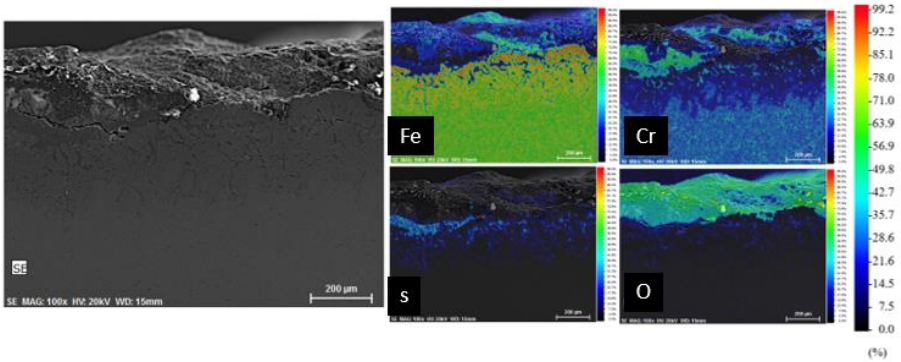

Fig. 54 Image of SEM and EDS quantitative mapping near the exterior surface (Sample 3-3)

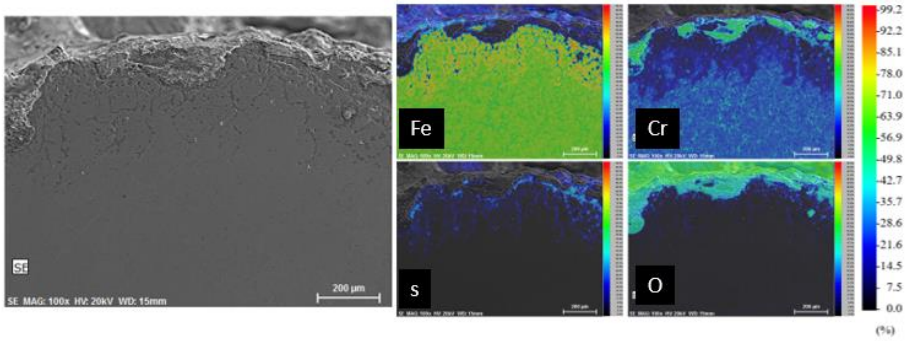

Fig. 55 Image of SEM and EDS quantitative mapping near the exterior surface (Sample 3-4)

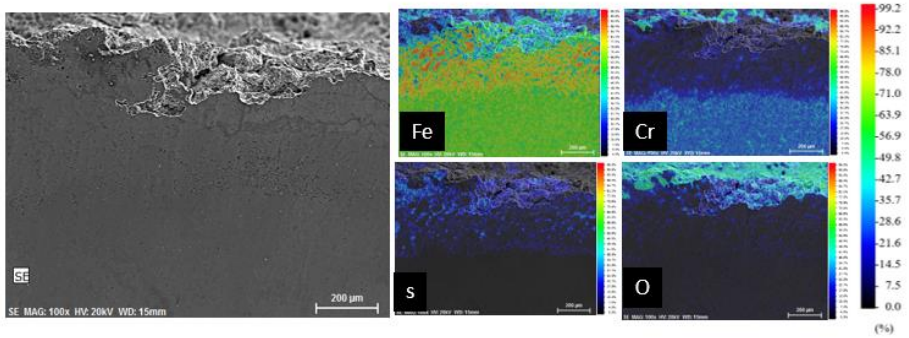

Fig. 56 Image of SEM and EDS quantitative mapping near the exterior surface (Sample 3-5)

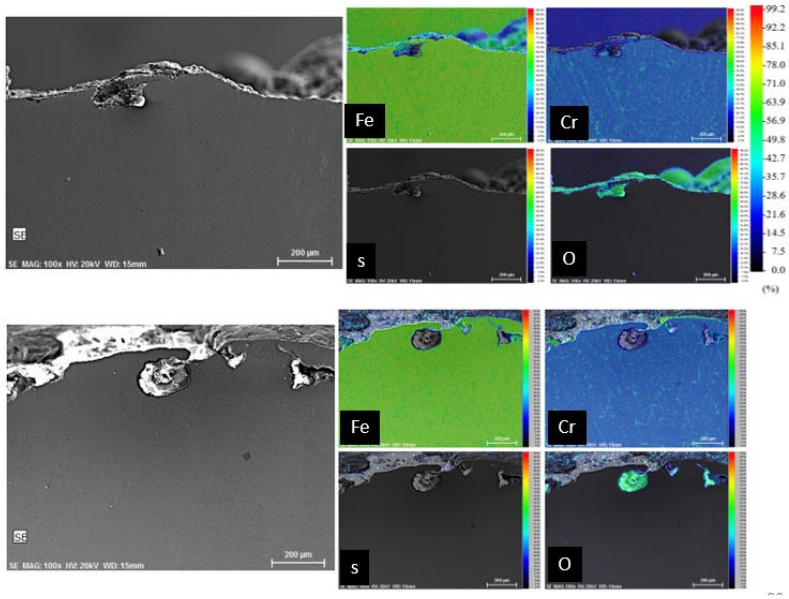

Fig. 57 Image of SEM and EDS quantitative mapping near the exterior surface (Sample 3-6 and 3-7)

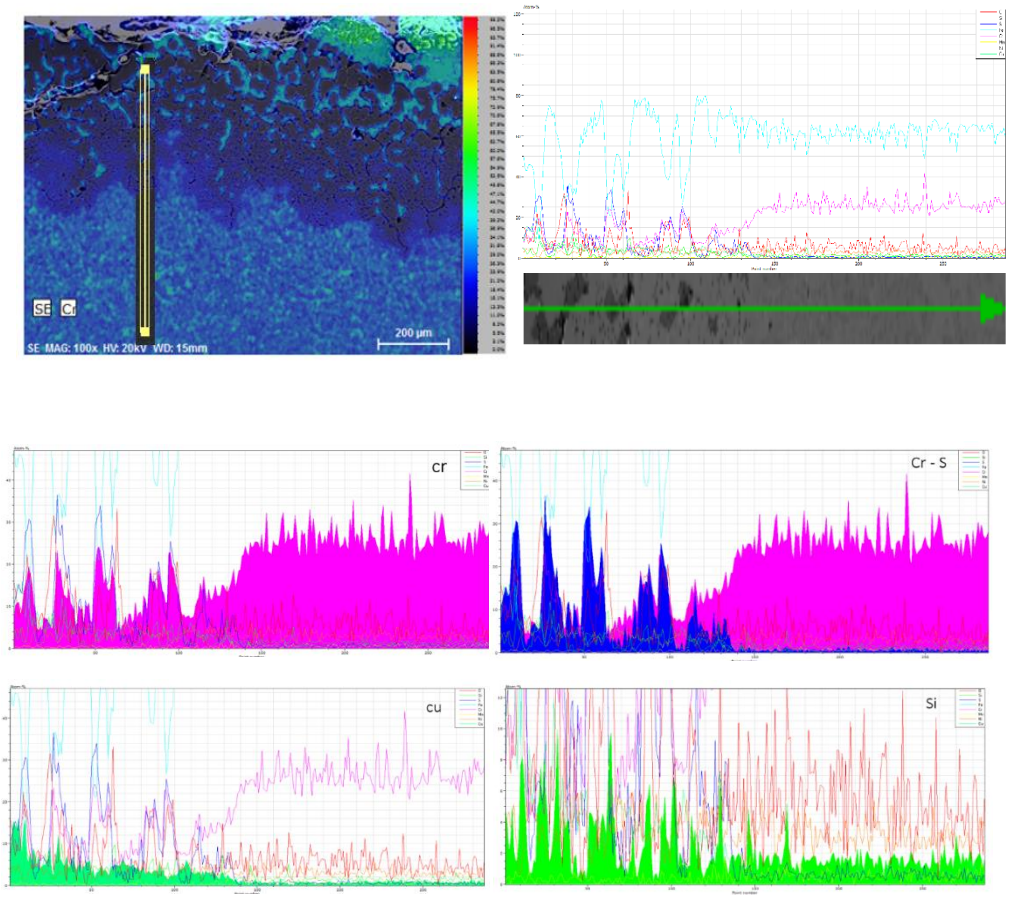

Fig. 58 Distribution of Cr, Cu, Si from line detection

After comparing the image with the part where chromium begins to maintain around 27%, (Fig. 58) it is the same as the start point of the boundary surface divided into dark and bright areas. The color-changing area on the image mean the last point where chromium is evaporated. (Fig. 59)

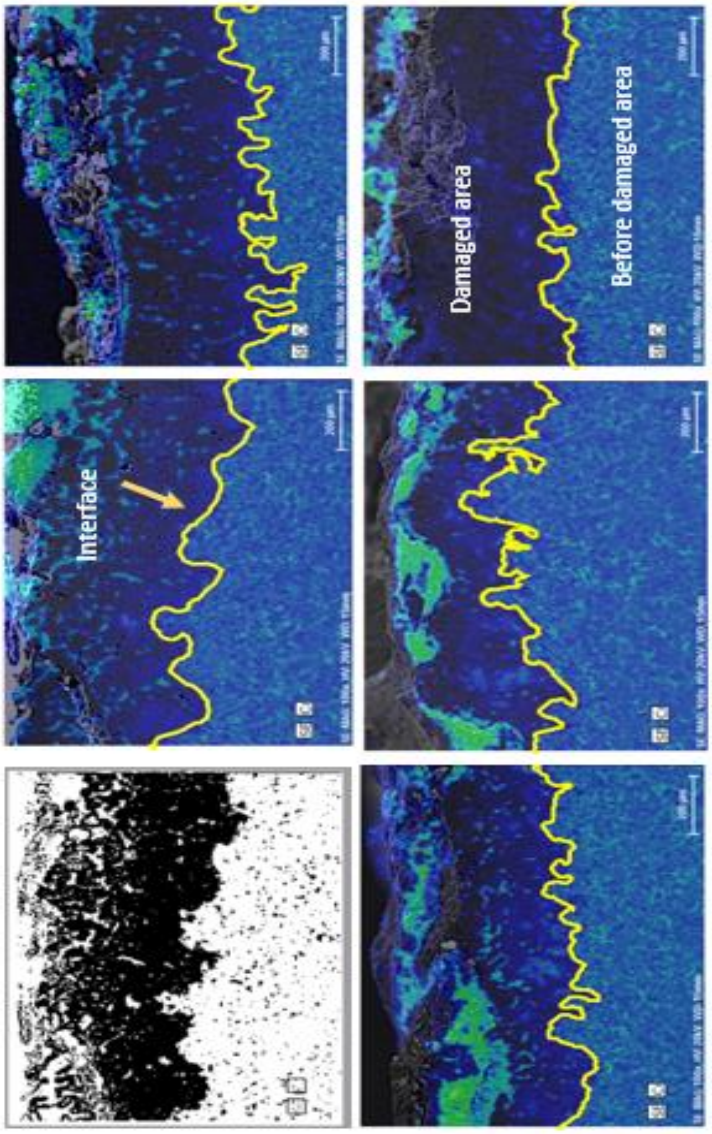

Fig. 59 Interface of damaged area and before damaged area with Metlab

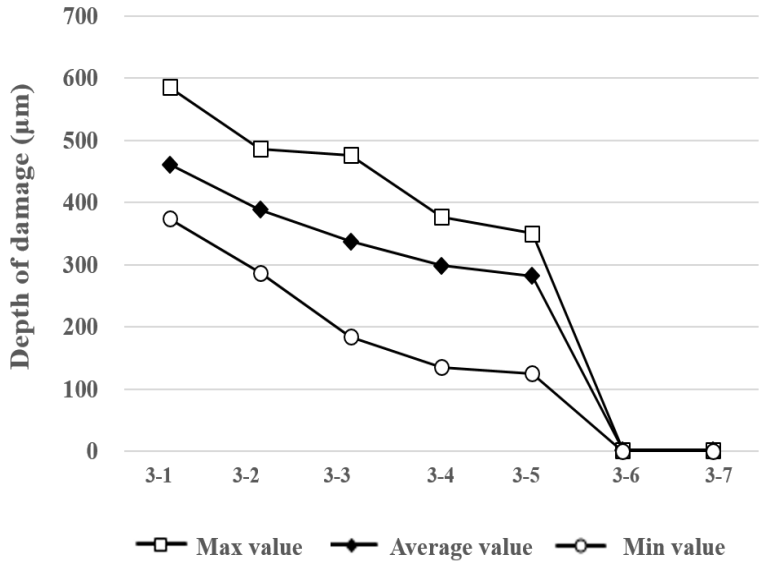

Fig. 60 Maximum, average, and minimum surface damage depth.

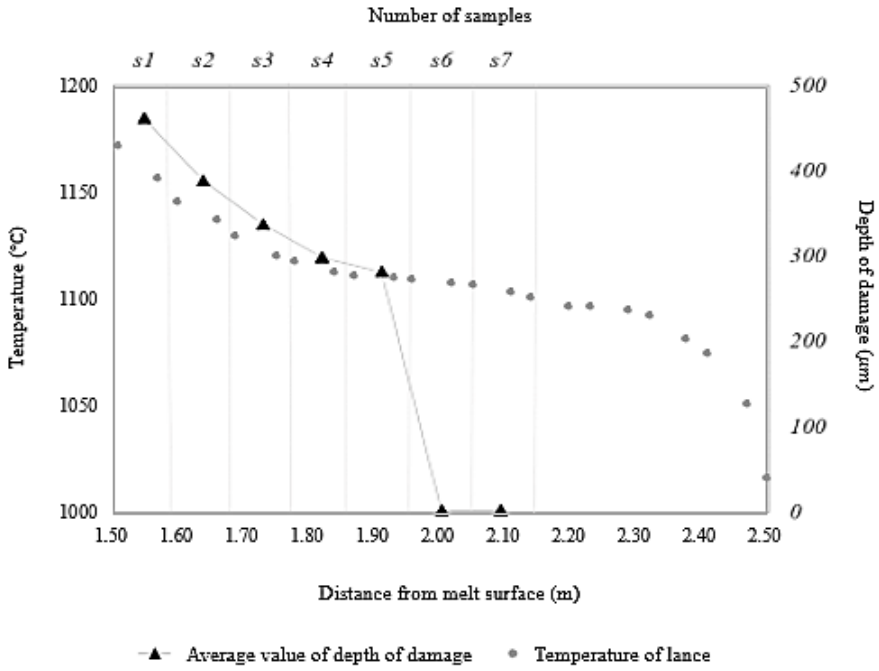

Fig. 61 Distribution of lance temperature and average value of surface damage depth.

Fig. 60 shows the average, maximum, and minimum values of the depth of damage for each sample and clearly shows that the depth of damage decreases as the height increases. Especially between samples 3-5 and 3-6, the values were sharply reduced and the damage rarely occurred in the top two samples. Results from the calculation showed the sequential decrease of lance temperature as height increases. (Fig. 61) This result shows different aspect with the result of damage depth from experiments and the micro-structure analysis contrastingly shows that there is no surface damage above a certain height. Hence, the effect of the temperature at the intersecting section is critical, furthermore, we can suggest from computational analysis that maintaining the lance height above 2m from melt surface to reduce lance fracture.

4.3. High magnification analysis

EDS mapping with a high magnification was conducted to analyze the components in the damaged area specifically. The compositions of the A, B and C regions in Fig 62 are listed in Table 5. Region A is composed of a Cu-Fe alloy, primarily consisting of Cu. Region B is comprised of CrS – CuS and region C contained an Fe-rich alloy which rarely contains Cr. Although Cu is not a lance component, it exists in the damaged area. Cu comes from matte because the following reactions can occur in the smelting furnace [20]

Numerical simulations showed that the matte and slag were forcefully splashed because of high speed gas and particle injections. [22] Thus, splashes of matte and slag can be attached to the lance surface during the process and can react to the lance.

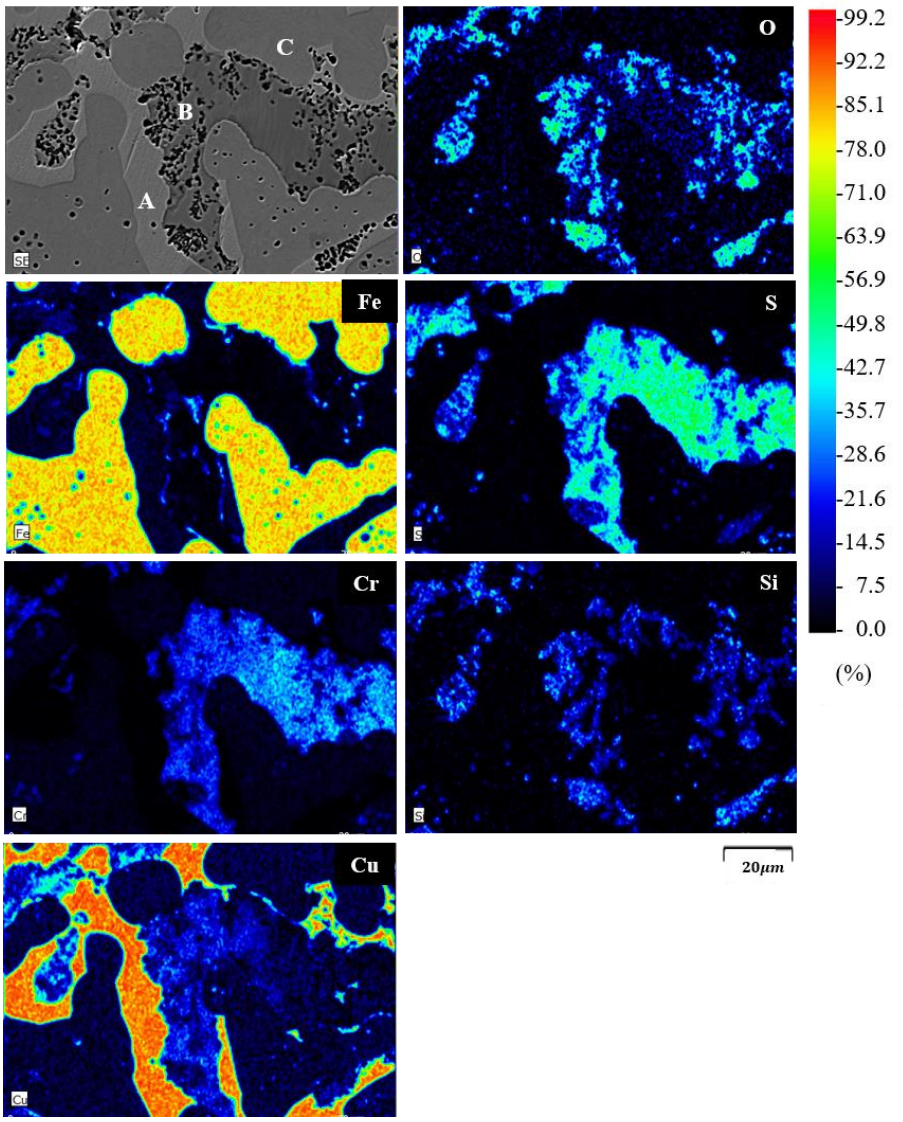

Fig. 62 Quantitative mapping of magnified EDS images of the damaged area of sample 3-2 for O, S, Fe, Cr and Cu in high magnification

(wt%)	Fe	Cr	Cu	S	O	Si	Ni	Mo	Mn
A	7.3	1.5	83.9	0.0	1.9	2.2	3.2	0.0	0.0
B	0.8	24.9	22.5	44.6	2.9	0.0	0.0	4.4	0.0
C	72.7	2.2	8.9	0.0	5.5	7.7	2.6	0.0	0.4

Table 5 Elemental composition (wt%) of Regions A, B and C

4.4. Thermodynamics calculations

From EDS mapping with a high magnification was conducted to analyze the components in the damaged area specifically. Region A is composed of a Cu-Fe alloy, primarily consisting of Cu. Although Cu is not a lance component, it exists in the damaged area. Cu comes from matte because the following reactions can occur in the smelting furnace.

$$CuFeS_2 + O_2 + SiO_2 \rightarrow (Cu_2S - FeS)_{matte} + (FeO\text{-}SiO_2)_{slag} + SO_2\,(g) \quad (21)$$

$$(Cu_2S)_{matte} + (Cr)_{matte} \rightarrow 2Cu + CrS \quad (22)$$

Numerical simulations showed that the matte and slag were forcefully splashed because of high speed gas and particle injections. [22] Thus, splashes of matte and slag can be attached to the lance surface during the process and can react to the lance.

First, since copper is contained in the mat in the melt, it tries to understand the reaction between Cu2S, the main component of the mat, and chromium in the lance. First, in order to analyze the affinity between the respective compositions first, copper, yellow and chromium are calculated by substituting them. As a result, although copper is partly solidified, it is confirmed in all temperature sections that chromium and sulfur are very close to each other.

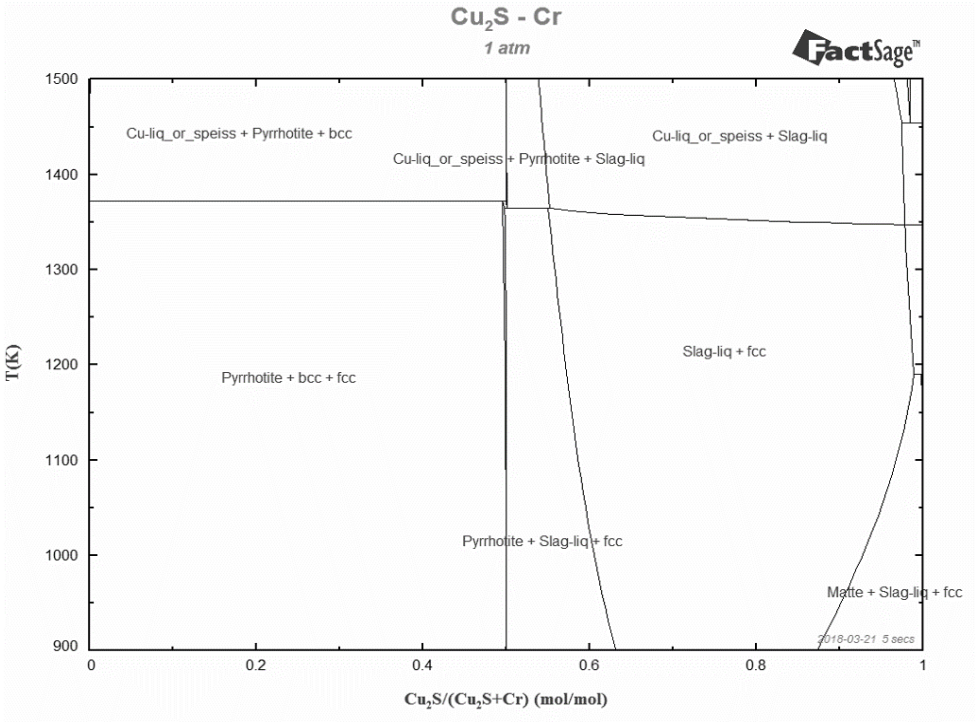

Fig. 63 Cu_2S-Cr

However, since actual copper and sulfur exist as Cu2S, they should be calculated by substituting the actual mat component instead of each composition. (Fig. 63) As a result of the calculation, chromium sulfide still exists over the entire region, and copper exists independently on the FCC. At that time, an important thing is a state at a high temperature. Although the composition varies, it was confirmed that copper, which existed almost purely at 1060-1090°C or higher, is melted and exists in a liquid state. High temperature odor potential is presented. High-temperature odors mean that when the river is heated to 1,000°C or higher, low-melting impurities such as iron sulfide, iron oxide and copper melt and soften the bond force of crystal grain boundaries, which causes hot cracks. In other words, the pure copper in the lance reacts with the mat can act as a cause for deteriorating the properties of the material.

An upper thermodynamic calculation result explains the same result as that of EDS Mapping, and since the more copper is provided by the splashing melt, the more likely it is to produce pure molten copper in the material, the greater the effect of splash on the material can be known, and at the same time, when a certain temperature condition is satisfied, the negative effect of copper in the material can be explained.

We are trying to explain not only that copper exists almost purely but also that it exists in a region completely different from chromium sulfide. The position where copper exists is the FCC region based on lance before use. Since copper is on FCC, it is expected to move through the FCC region in the dual phase of the conventional lance. To confirm this thermodynamically, a thermodynamic

calculation was made for the formation by temperature. The percentage of each prize varies depending on the temperature. Therefore, the FCC and BCC ratios could not be identified as one. So we calculated the FCC and BCC rates and mat reactions that vary depending on the temperature, and we calculated intensively for nearly 1100 degrees Celsius where copper melts.

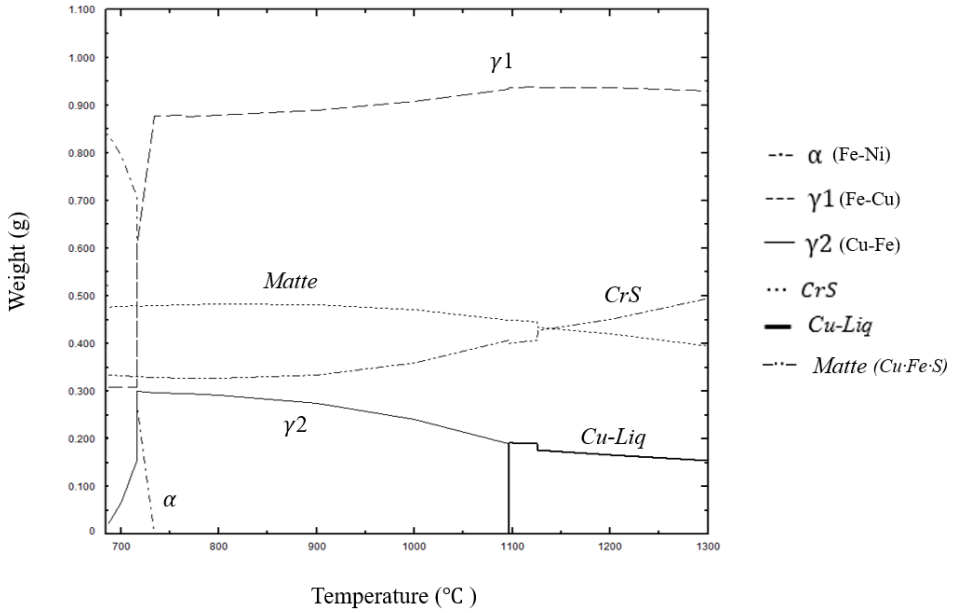

Fig. 64 Fact-sage result for the reaction between lance and Cu_2S-FeS

To determine the reaction in the lance with matte, thermodynamic calculations were executed from the Equilib module of FactSage. And PS (Pure substance) database, misc (Miscellaneous compounds) database and the stel (steel alloy) database was used. Fig. 64 shows the results of the reaction of the matte and lance compositions at different temperatures. Different phases can form at different temperatures. Numerical simulations showed that the temperature range of lances in the smelting furnace was between 800℃- 1200℃. [22] γ_1 (mainly Fe), matte, and CrS phases appear in this temperature range. However, a phase with a high concentration of Cu exists as a liquid at temperatures above 1098℃ and as a solid state(γ_2) below that temperature. This Cu- rich phase of region B in Fig.62 might be formed by the substitution of Cr to Cu in the matte. $(Cr + Cu_2S \rightarrow CrS + 2Cu)$. The CrS coexists near the matte, and region A of Fig.62 was comprised of these mixed phases. The remaining Cr- depleted phase might be the phase of region C in Fig.62. The shape of Cu rich phases prolonged into the bulk of lance. This Cu - rich metal phases were not observed in sample 2.

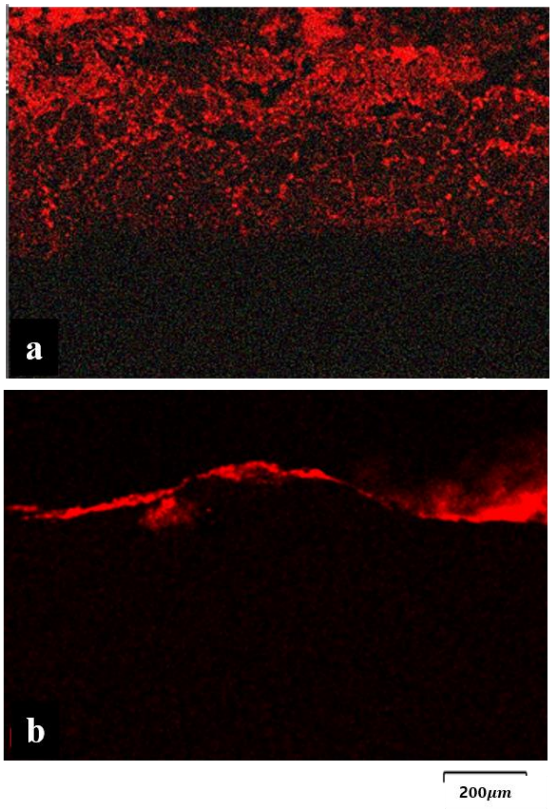

Fig. 65 Images of SEM and EDS mapping on (a) sample 3-5 (b) sample 3-6

To identify the effects of the Cu-rich phases, the Cu distribution in sample 3-5 and 3-6 was studied. Two samples were taken from adjacent locations; however, the damage depth of sample 3-6 was much smaller than that of sample 3-5. Fig. 65 shows that Cu is penetrated into the damaged surface of the lance in sample 3-5. On the other hand, Cu existed only near the surface of the lance in sample 3-6. At any temperature, Cr reacts with Cu_2S to form Cu and CrS. When the temperature is higher than 1098℃, thermodynamic calculation shows that the Cu forms Cu-rich liquid phase. On the other hand, if temperature is lower than 1098℃, Cu forms γ_2 solid. The formation of the liquid phase could change the reaction kinetics, as shown in Fig.66. The reaction between CuS and Cr in metal occurred at the interface between matte and metal. When temperature is lower than 1098℃, solid phase of Cu-rich metal forms and further reaction can proceed after Cr diffuse at this new barrier. This barrier can slow down the proceeding of the reaction as shown in Fig.66. On the other hand, when temperature is higher than 1098℃, the Cu-rich phase is liquid, so the liquid phase forms droplet to decrease surface tension. Therefore, barrier is not formed between metal and matte. Because of that the reaction can proceed continuously. Furthermore, the liquid Cu phase can penetrate Cu to grain boundaries and can cause thermal brittleness. [27-28] The large difference of damage depth between lower part (sample 3-1 - 3-5) and upper part (sample 3-6 and 3-7) can be explained the formation of Cu liquid at the lower part. And the formation of liquid Cu could be the main cause of frequent fracture of lances in smelting furnaces of the Mitsubishi continuous process.

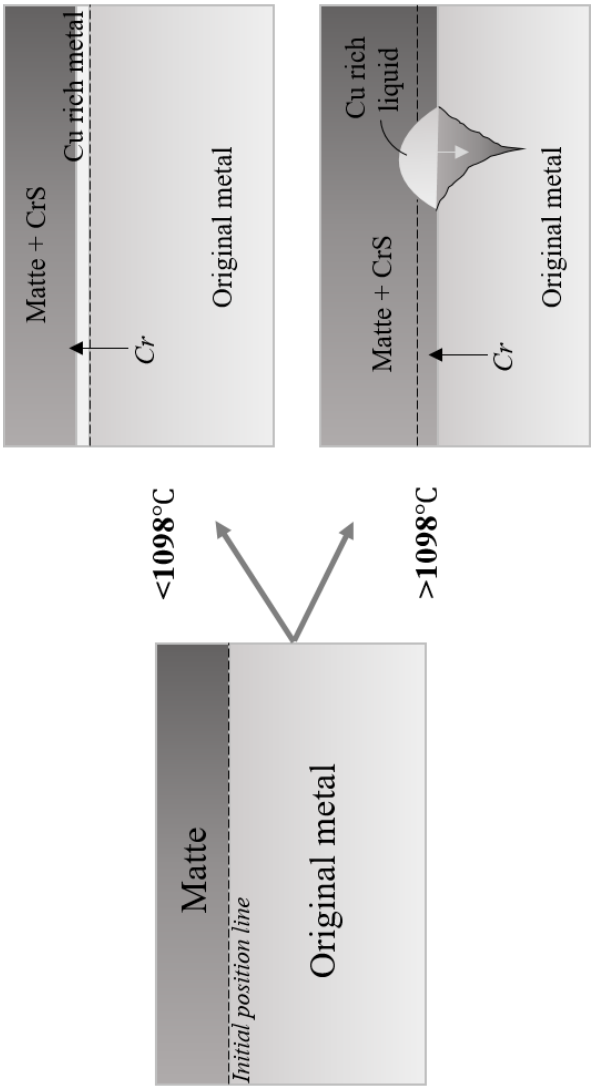

Fig. 66 Images of mechanism of reaction

4.5. Laboratory experiments

4.5.1. Conditions of lab experiments

Thermodynamic calculations using Fact-sage showed that if the temperature is above 1098℃, the liquid phase appears. To confirm this prediction, laboratory experiments were performed with lance materials and matte gathered during field operations.

Lab experiments were conducted by creating the same environment as the lance is used in smelting furnace. (Fig. 67) We used unused-lance and powder of matte which is collected from smelting furnace then grinded it finely. The matte powder was placed on crucibles. The exterior of the lance sample was put on top of the matte and placed facing the crucible bottom for the continuous supply of matte. Hydrogen gas was injected to create a reducing atmosphere and kept at a given temperature for 8 hours in 1000 °C and 1100 °C respectively. The surface morphology and composition of the lance exterior was analyzed using micro-structure analysis. The interface between the lance sample and matte attached after heat treatment was selected as the analysis area.

Fig. 67 Methods of experiments

4.5.2. Condition1: 1000℃

The individual figures can be divided into two areas (lance region and matte region). (Fig. 68) The microstructure observation shows that the Cu, S, and oxygen (O) only attached to the lance that contained Fe and Cr. Cu did not penetrate the sample, verifying that the splashed matte (Cu-Fe-S) and the lance did not react at a 1000 ℃.

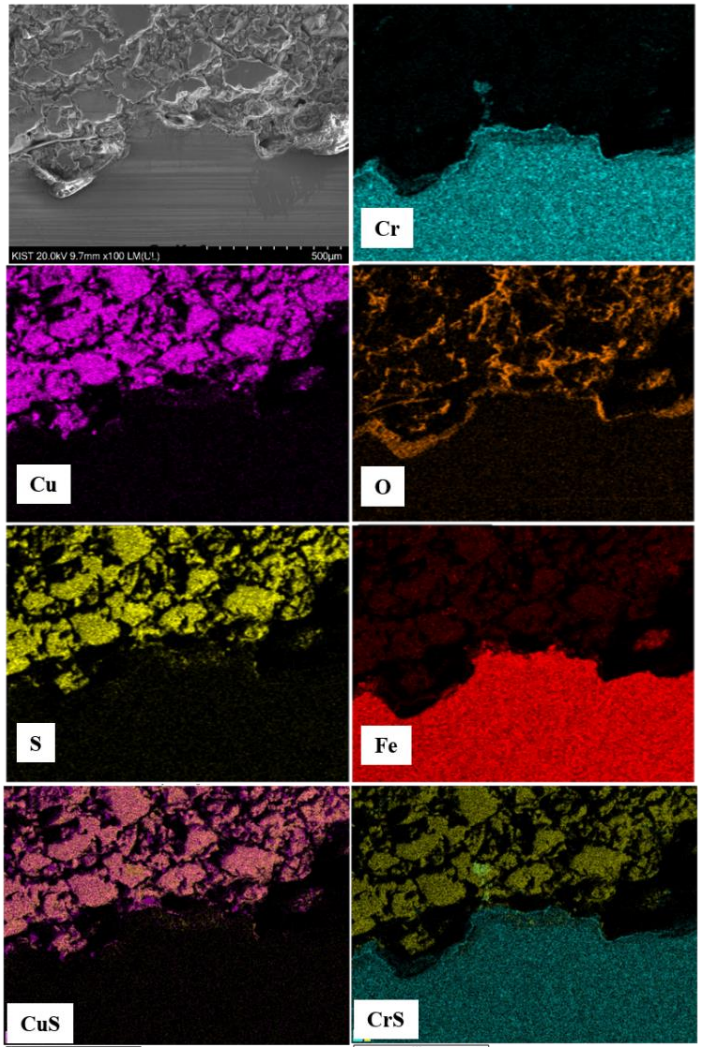

Fig. 68 Images of SEM and EDS quantitative mapping in low magnification at 1000 °C.

4.5.3. Condition2: 1100℃

the interface between the lance and the attached matte that is not separated at 1100 ℃, leading to the Cu and S penetrating through the damaged area. Furthermore, the penetrated S exists in the same area as the Cr. (Fig. 69) These results differ from the results obtained at a 1000 ℃. The chemical composition of the points in a high magnification image was analyzed to obtain a more accurate comparison.

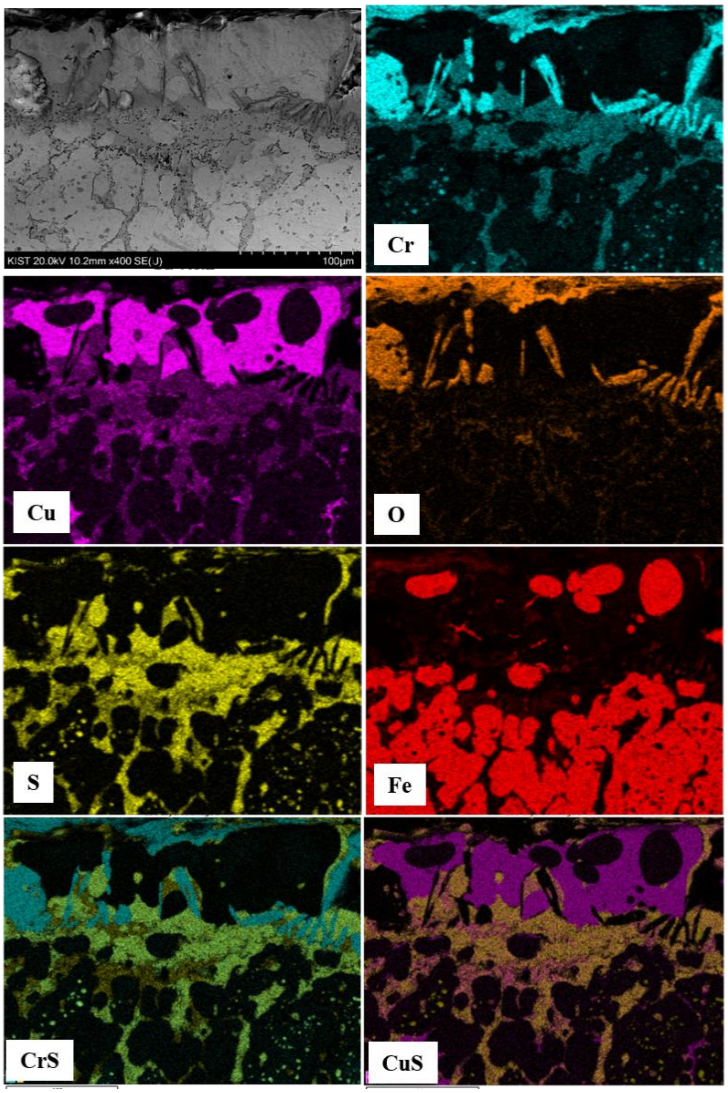

Fig. 69 Images of SEM and EDS quantitative mapping in low magnification at 1100 °C.

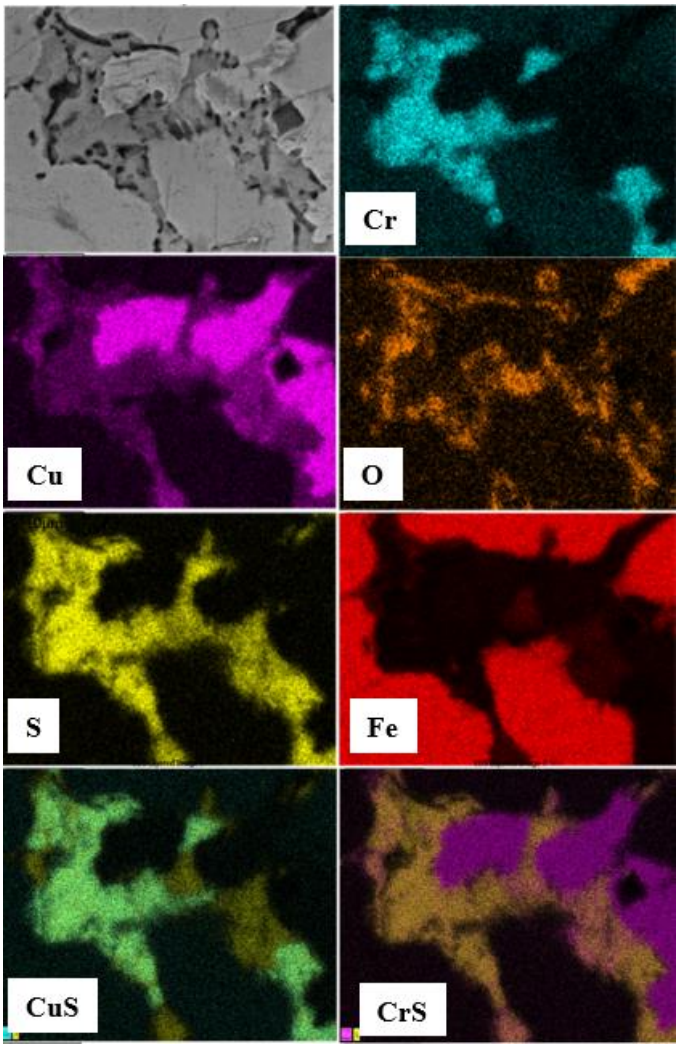

Fig. 70 Images of SEM and EDS quantitative mapping in high magnification at 1100 °C.

The results are similar to the results obtained from the field operation experiment (Fig. 62). Fig. 70 also can be divided into three regions: Region A, where Cu exists; Region B, comprising of chromium sulfide precipitation (CrS); and Region C, which is the lance region. The composition of each region was analyzed (Table 6). And this result also can be interpreted as a result that the molten matte reacted with the lance and penetrated into the lance surface then copper alloy and CrS. In other words, the experimental laboratory results are similar to the micro-structure analysis and thermodynamic calculated results and we confirmed that the critical temperature was near 1100 ℃.

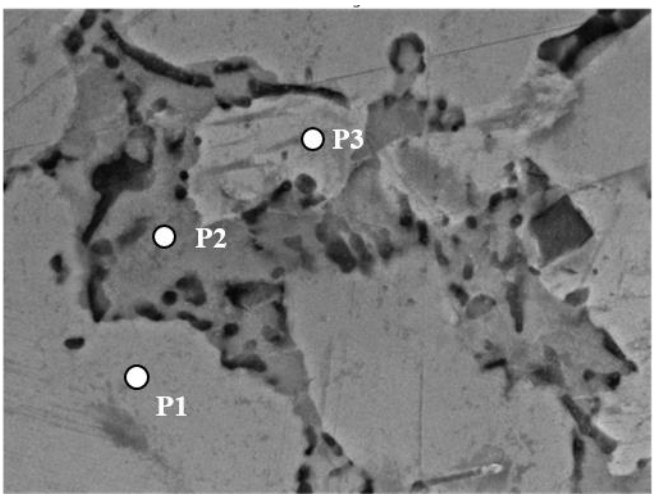

Fig. 71 SEM Images in high magnification at 1100°C.

Element (wt%)	P1	P2	P3
O	0.38	0.77	0.55
Si	0.15	0.12	0.16
S	0.31	**34.40**	0.21
Cr	2.61	**25.73**	0.53
Fe	**88.21**	5.50	4.91
Cu	8.34	**33.49**	**93.65**
Total:	100.00	100.00	100.00

Table 6 Chemical composition of points.

4.5.4. Condition3: 1090℃

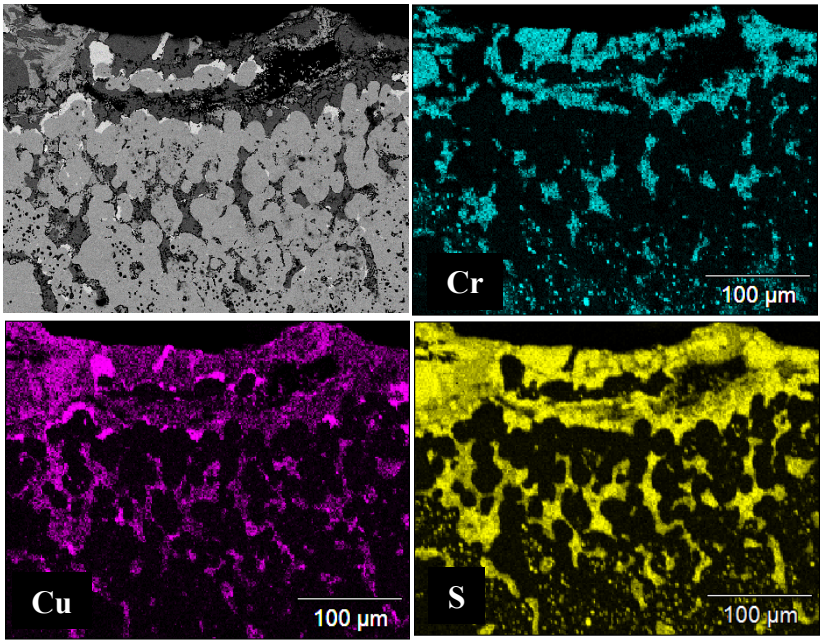

Fig. 72 Images of SEM and EDS quantitative mapping in low magnification at 1090 °C.

From the thermodynamics calculation (Fig. 64), the temperature at which the liquid copper is produced is just under 1100℃, 1098℃. (Fig. 72) So the reaction of the matte and lance was analyzed at 1090℃ through additional laboratory experiment. In Fig.73, the SEM and EDS quantitative mapping in high magnification show that Cr existed with S as precipitations in places and Cu and S located in similar positions with Cr which has similar composition with P1 in Fig. 73. This region was comprised of chromium sulfide and copper sulfide (CrS - CuS). (Table 7) And this result can be interpreted as matte was penetrated into lance but in this temperature, lower than 1100℃, liquid copper did not melt out from region with CrS - CuS.

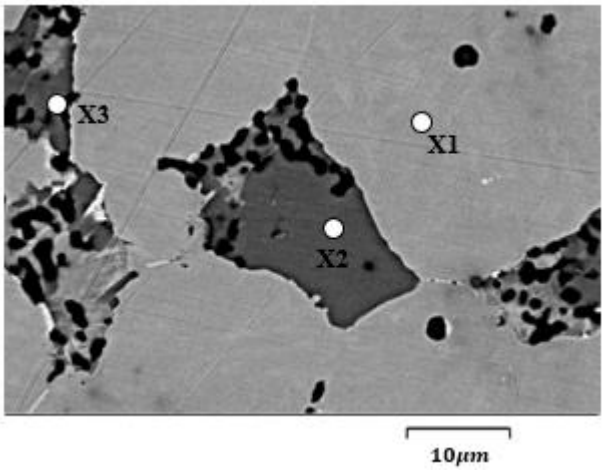

Fig. 73 Images of SEM and EDS quantitative mapping in high magnification at 1090 °C

Element (wt%)	X1	X2	X3
O	0.00	0.00	0.00
Si	0.07	0.00	0.16
S	0.00	32.12	31.55
Cr	2.17	26.56	25.82
Fe	89.39	2.84	3.56
Cu	6.69	36.03	35.49
Total:	100.00	100.00	100.00

Table 7 Chemical composition of points.

From our lab experiments, we found that temperature effect on fracture of lance phenomena. Lance did not deteriorate in 1000°C but in 1090°C, surface was damaged and matte was penetrated and reacted with lance because difference of temperature had decisive effect on reaction rate. However liquid copper was produced as well as matte and lance reacted in 1100°C experiment. The liquid is known to progress rapidly in general. Liquid copper could penetrate quickly along the damaged grain boundary. We confirmed through this experiments that because liquid copper exists in high temperature, fracture of the lance can easily occur in the given environment of smelting process.

4.5.5 Summary

The results of the present experiments and thermodynamic analysis showed that the main mechanism of frequent fracture of lances in smelting furnace is the formation of the liquid Cr-rich phase by the reaction between the matte and lance at high temperatures. The liquid phase can be formed at temperatures above 1100℃. Therefore, the part of the lance located at higher temperatures than 1100℃ quickly reacted with the matte, deteriorated and finally fractured. Based on the experimental results, laboratory experiments were conducted and liquid copper was also produced at above 1100℃. From this results, it can be deduced that temperature above 1100℃ can cause the lance fracture and part of the lance located at higher temperature than 1100℃ can be deteriorated and finally fractured. This means that if we want to extend lance life, the lance temperature must be lower than 1100℃ to prevent the reaction between the matte and lance materials.

Chapter 5. Conclusions

This study was focused on the extension of the lance life in the smelting furnace of the Mitsubishi process. To study the phenomena in the furnace, we developed numerical analysis models, calculated the transport phenomena using the models, and conducted field experiments. The numerical simulation showed that the lance height considerably influences the transport phenomena in the furnace and suggested that the lance failure could be decreased by raising the position of the lances since it could reduce the temperature of the lances. Based on the simulation results, the smelting furnace process was performed with a higher lance position. The number of lances consumed and concentrations of weak-acid were monitored to determine the effects of the change in the lance positions. The results indicated that the number of consumed of lances decreased by approximately 50%, and the concentrations of the weak-acid were nearly equivalent in both the original and modified lance height conditions. Thus, it could be concluded that the use of the modified operating condition could decrease lance failure without a loss of the reaction ability of the smelting furnace. Further, it is indicated that the feeding system is a method for stabilizing the inside of the furnace during the process. At present, injection materials are fed crosswise, but when the feeding system was changed to continuous feeding, the flow velocity in the furnace was generally stabilized and the lance temperature could be maintained relatively low. In addition, when concentrates and gas are continuously injected into all lances, the probability of establishing the preconditions of bath smelting increases and the unreacted

oxygen is reduced. Therefore, the values of reaction area were compared and suggested that continuous feeding system is more stable for process.

And present study also focused on figuring out the cause of lance fracture in a smelting furnace of the Mitsubishi process. The microstructure of lance samples from the field operations was analyzed. The structure of samples was damaged to a certain height and elements such as Cu, O and S penetrated to the lance along the damaged grain. The damaged area was divided into Cu-Fe alloy and CrS-CuS as splashed matte and lance reaction occurred. For analyzing this reaction, thermodynamics were calculated using Fact-sage and the Cu-Fe alloy existed as a liquid phase at approximately 1100℃. Based on the experimental results, laboratory experiments were conducted and liquid copper was also produced at above 1100℃. From these results, it can be deduced that temperature above 1100℃ can cause the lance fracture and the part of lance located at higher temperature than 1100℃ can be deteriorated and finally fractured. Thus, during the Mitsubishi process, when the lance is kept at a temperature below 1100 in the furnace, the surface damage can be reduced and the lance life-time can be increased.

References

[1] Etsuji Kimura, “Fundamental research of lancing mechanism in Mitsubishi continuous smelting furnace”, ISIJ, 23, p. 522-529. (1983)

[2] M. Goto, E. Oshima, and M. Hayashi., “Control aspects of the Mitsubishi continuous process”, JOM April, p. 60-64. (1998)

[3] T. Utigard, J. M. Toguri, and T. Nakamura, “Interfacial tension and flotation characteristics of liquid metal-sodium flux systems”, Metallurgical Transactions B, 17B, p.339-346. (1986)

[4] W. G. Davenport, M. King, M, Schlesinger, and A. K. Biswas., Extractive metallurgy of copper, 4th edition, ELSEVIER Sci. Ltd., p. 57-72. (2002)

[5] M. Goto and T. Echigoya, “Effect of injection smelting jet characteristics on refractory wear in the Mitsubishi process”, J.Metals, 32 (11). (1980)

[6] S. -S. Park, N. Dyussekenov, and H. -Y. Sohn, “The penetration behavior of an annular gas-solid jet impinging on a liquid bath: Comparison with a conventional circular jet”., Metall. and Mater. Trans. B, 41B, p. 51-62. (2010)

[7] Y. -B. Hahn and H. -Y. Sohn, “Mathematical modeling of sulfide flash smelting process: Part I. Model development and verification with laboratory and pilot plant measurements for Chalcopyrite concentrate smelting”, Metal. Trans. B, 21B December, p.945-958. (1990)

[8] M. Nagamori, W. J. Errington, P. J. Mackey, and D. Poggi, “Thermodynamic simulation model of the Isasmelt process for copper matte”, Metal. and Mater. Trans. B, 25B December, p.839-853. (1994)

[9] X. F. Li and T. Xiao, “Production enhancement and operation parameter’s optimization of the flash smelting furnace based on numerical simulation”, CSIRO Australia, p.155-160. (2003)

[10] Young, D.J., Watson, S., 1995. High-Temperature Corrosion in Mixed Gas Environments. Oxid. Met, vol. 44, nos. 1/2.

[11] Asteman, H., Svensson, J.-E., Johansson, L.-G., 2002. Evidence for Chromium Evaporation Influencing the Oxidation of 304L: The Effect of Temperature and Flow Rate. Oxid. Met, vol. 57, nos. 3/4.

[12] Sahlaouia, H., Makhloufa, K., Sidhoma, H., Philibertb, J., 2004. Effects of ageing conditions on the precipitates evolution, chromium

depletion and intergranular corrosion susceptibility of AISI 316L: experimental and modeling results. Mater. Sci. Eng, A 372, 98–108.

[13] FLUENT Theory guide, Fluent Inc. (2013)

[14] Maksim Mezhericher, “Modeling of particle pneumatic conveying using DEM and DPM methods”, Particulate Sci. and Tech., 29, p.197-208. (2011)

[15] B. R. Cornard, R. Sridhar, and J. S. Warner, “High-temperature thermodynamic properties of chalcopyrite”, J. Chem. Thermodynamics, 12, p.817-833. (1980)

[16] J. J. Beazuidenhout, J. J. Eksteen, and S. M. Bradshaw, “Computational fluid dynamic modelling of an electric furnace used in the smelting of PGM containing concentrates”, Minerals Eng., 22, p.995-1006. (2009)

[17] M. Goto, The Mitsubishi continuous process - operation and design (Mitsubishi Materials Corporation, Tokyo, 1988).

[18] M. Goto and M. Hayashi, The Mitsubishi continuous process:

Metallurgical Commentary, 2nd edn. (Mitsubishi Materials Corporation, Tokyo, 2002).

[19] Lim, S.-M., Park, S.-S., Yi, K.-W. 2020. Extension of Lance Life by Change of Height of Lances in the Smelting Furnace of Mitsubishi Process. Met. Mater. Int. https://doi.org/10.1007/s12540-020-00712-x

[20] I.-K. Choi, Met. Mater. Int, 2, 245 (1996).

[21] R.D. Monteiro, J.V.D. Wetering, B. Krawczyk, D. Engelberg, Met. Mater. Int. (2019) htps://doi.org/10.1007/s12540-019-00403-2

[22] B.S. Bokstein, B. Straumal, Diffusion, Segregation and Stresses in Materials (Trans Tech Publications Ltd, 2003).

[23] Asteman, H., Svensson, J.-E., Johansson, L.-G., 2002. Evidence for Chromium Evaporation Influencing the Oxidation of 304L: The Effect of Temperature and Flow Rate. Oxid. Met, vol. 57, nos. 3/4.

[24] Sahlaouia, H., Makhloufa, K., Sidhoma, H., Philibertb, J., 2004. Effects of ageing conditions on the precipitates evolution, chromium depletion and intergranular corrosion susceptibility of AISI 316L: experimental and modeling results. Mater. Sci. Eng, A 372, 98–108.

[25] Shibata, K., Seo, S.-J., Kaga, M., Uchino, H., Sasanuma, A., Asakura, K., Nagasaki, C., 2002. Suppression of Surface Hot Shortness due to Cu in Recycled Steels. Mater. Trans, vol. 43, no. 3, 292-300.

[26] Savage, W.F., Nippes, E.F., Mushala, M.C., 2013. Liquid-Metal Embrittlement of the Heat Affected Zone by Copper Contamination.